https://doi.org/10.5194/esurf-2022-66
Preprint. Discussion started: 5 December 2022

Earth Surface Dynamics Discussions
Open Access
EGU

6

Impacts of Human Modifications on Material Transport in Deltas

Jayaram Hariharan[1], Kyle Wright[1], Andrew Moodie[1], Nelson Tull[1], and Paola Passalacqua[1]

[1]Department of Civil, Architectural and Environmental Engineering, Center for Water and the Environment, University of Texas at Austin, Austin, Texas, USA

Correspondence: Paola Passalacqua (paola@austin.utexas.edu)

Abstract. As humans continue to inhabit and modify river deltas, the natural processes governing material transport through these landscapes are altered. Two common engineering projects undertaken on deltas are the dredging of channels to enable shipping and the construction of embankments to reduce flooding. While the impact of these topographic modifications has been studied at a local-level for specific sites, there is a gap in our generalized understanding of how these landscape modifications impact material transport. To narrow this gap, we conduct exploratory numerical modeling to develop deltaic landscapes with different input sediment compositions, modify their topography to mimic dredging and embankments, simulate different flow conditions, and then model the transport of passive particles. We find that human modification of topography lowers hydrological connectivity by reducing the area visited by fluvial inputs. The amount of time particles spend within the delta is reduced by the construction of polders and is lengthened by dredging. Material buoyancy has a greater impact on nourishment areas and exposure times than flow regime or topographic modification, with positively-buoyant particles spending longer and visiting a greater area of the delta than neutral and negatively-buoyant material. The results of this study can help guide the design of future engineering projects by providing estimates of their likely impact on transport processes.

1 Introduction

Humans have chosen to inhabit delta landscapes for centuries due to their coastal locations and nutrient-rich soils (Day et al., 2007; Edmonds et al., 2020). To increase the habitability of these dynamic landscapes, humans have enacted a number of topographic modifications, such as levee construction and channel dredging, to promote stability. Not unlike upstream construction (e.g., dams, Higgins et al., 2018), these efforts to control nature alter the processes occurring on the landscape (e.g., Simeoni and Corbau, 2009; Renaud et al., 2013; Wilson et al., 2017), and reduce long-term sustainability (Passalacqua et al., 2021). These disruptions to natural transport mechanisms within deltas can result in the loss of flora and fauna (e.g., Ohimain, 1996; Ellery and McCarthy, 1998).

Embankments, or levees, are constructed to limit erosion and prevent low-lying land from flooding (e.g., Samuelson, 1917; Le et al., 2007; Renaud et al., 2013; Olson and Wright Morton, 2018). Unfortunately, embankments also prevent the delivery of sediment to the floodplains and interiors of deltaic islands, which in the presence of land subsidence and in-channel sedimentation, can lead to geomorphically unstable situations wherein the adjacent channel bed is higher than the land behind the embankment (e.g., Auerbach et al., 2015). This type of instability has resulted in a number of alternative practices, including

https://doi.org/10.5194/esurf-2022-66
Preprint. Discussion started: 5 December 2022


Earth Surface Dynamics Discussions
Open Access
EGU

''soft'' flood-risk management (Wesselink et al., 2015), and the adoption of nature-based engineering solutions (Temmerman and Kirwan, 2015). In Bangladesh, for example, the intentional breaching of embankments to allow sedimentation to occur, a process called tidal river management, partially restores the landscape by allowing water and sediment to flood the island interior during the rainy season (e.g., Khadim et al., 2013; Masud et al., 2018; Al Masud et al., 2020).

The artificial deepening of channels via dredging to enable shipping and commerce is another typical human engineering practice (e.g., Ohimain, 1996; Day et al., 2000; Yuan and Zhu, 2015). This channel deepening can promote imbalance between shallow and deep parts of the system leading to decreased channel dynamics (van Dijk et al., 2021). These morphological changes can lead to the destruction of aquatic fauna (Ellery and McCarthy, 1998), as well as the enhancement of pre-existing oxygen deficiencies (Kerner, 2007). Dredging can also change flow behavior, altering the partitioning of flow at upstream junctions (e.g., Yuan and Zhu, 2015), as well as increasing the tidal range (Cai et al., 2012; Yuan and Zhu, 2015; Zhu et al., 2015), thus making coastal areas more vulnerable to storm surge (Cai et al., 2012).

The movement of water and sediment between channels and their floodplains is more broadly a type of hydrological connectivity. Hydrological connectivity describes the water-mediated transport of material between landscape elements (Pringle, 2003; Tetzlaff et al., 2007; Lexartza-Artza and Wainwright, 2009). Beyond water and sediment, the concept of hydrological connectivity can be applied to nutrients, pollutants, or any other material being transported through a landscape (Passalacqua, 2017). Within natural river deltas, hydrological connectivity has been found to be both significant (Hiatt and Passalacqua, 2015) and important to the natural functioning of the landscape (Hiatt et al., 2018; Christensen et al., 2020; Olliver and Edmonds, 2021).

Deltas themselves can have drastically varied morphologies due to differences in fluvial inputs of water and sediment, wave environments, tidal signals, and climatic conditions (e.g., Galloway, 1975; Caldwell and Edmonds, 2014; Anthony, 2015; Piliouras et al., 2021). These environmental conditions lead to variations in morphology, which subsequently create unique hydrodynamic and sediment transport behavior (e.g., Sassi et al., 2011). Sediment composition, for example, influences both delta morphology and dynamics. Finer-grained cohesive sediments lengthen avulsion timescales, resulting in the formation of rugose shorelines, while coarser-grained sediments have more mobile channels and smoother, fan-like, shorelines (Hoyal and Sheets, 2009; Edmonds and Slingerland, 2010; Caldwell and Edmonds, 2014; Straub et al., 2015). Consequently, material transport through natural river deltas is expected to vary based on morphology and environmental forcings. Human modifications to these natural systems may alter transport behavior leading to reduced, or increased, connectivity between landscape elements. For example, the embankment of land has been shown to lead to amplification of local tidal signals, changing both the morphology of tidal channels and the connectivity of the landscape (Pethick and Orford, 2013; Auerbach et al., 2015; Bain et al., 2019).

Numerical simulation of different coastal locations, ports, and channels, has enabled some quantification of material transport in the face of human modifications (e.g., Proehl et al., 2004; Banas et al., 2009; Vale and Dias, 2011). Sometimes these studies are performed in advance of a proposed engineering project to assess its environmental impact (e.g., Valseth et al., 2021). Other times studies are done after engineering projects are complete, providing an evaluation of their impact (e.g., Day et al., 2000; Monge-Ganuzas et al., 2013; Yuan and Zhu, 2015). The generic impact of human topography modifications on material

https://doi.org/10.5194/esurf-2022-66
Preprint. Discussion started: 5 December 2022


Earth Surface Dynamics Discussions
Open Access
EGU

transport through river delta landscapes, however, is relatively understudied. Developing this type of generalized knowledge about the changes in transport behavior due to topographic modifications can be applied to inform future studies.

In this work, we explore the impact that embankment construction and channel dredging have on material transport in river delta environments via the use of numerical models. First, we simulate the evolution of natural river deltas with different input sediment compositions over a period of 150 years. Next, we modify the modeled ''natural'' topography to mimic channel dredging and island embankment, and evaluate changes to flow and transport over timescales on the order of days. We simulate bankfull discharge at the inlet flowing into a receiving basin with and without a micro-tidal signal, and use a Lagrangian framework to simulate the transport of material through the different landscapes under the modeled flow conditions. We compare model results to understand how different natural conditions (sediment composition), topographic modifications (dredging, poldering), and flow conditions (no-tides, tides), influence the transport of material through the landscape.

2 Methods

2.1 Landscape Modeling

To generate deltaic landscapes, we use the reduced-complexity model `pyDeltaRCM` (Moodie et al., 2021). Based on the original DeltaRCM model (Liang et al., 2015), `pyDeltaRCM` simulates the inception and growth of a river delta from an inlet channel through which a steady flow of water and sediment enters a receiving basin. We simulate reduced-complexity hydrodynamics and sediment transport processes using discrete quantities of water and sediment which move through the domain via a series of weighted random walks, with weights calculated based on physically-based rules (Liang et al., 2015). This methodology enables deltaic evolution to be simulated over hundreds of years under different forcing conditions (e.g., Liang et al., 2016b, a; Lauzon and Murray, 2018; Lauzon et al., 2019; Piliouras et al., 2021; Hariharan et al., 2021; Moodie and Passalacqua, 2021).

In this work we simulate delta evolution over a period of 150 years (Figure 1). We scale modeled bankfull time using an assumption of 10 bankfull days per year to obtain an equivalent scaled time of 150 years (Caldwell and Edmonds, 2014; Liang et al., 2016b; Lauzon and Murray, 2018; Lauzon et al., 2019). The basin dimensions (Figure 4a), model parameters, and simulation duration are based on Liang et al. (2016b) and have been applied in other studies which use the same modeling approach (e.g., Lauzon and Murray, 2018; Lauzon et al., 2019). Sediment is divided into two classes in the `pyDeltaRCM` model: sand, representative of coarse grain material, and mud, representative of fine grain material. The composition of sediment introduced to the system, expressed as a sand fraction (f_{sand}), influences both surface morphology, channel mobility, and sediment arrangement in the subsurface (Liang et al., 2016b; Hariharan et al., 2021). In this work we simulate three input sand fractions (0.25, 0.5, and 0.75) and repeat each numerical experiment six times, to obtain results representative of average ensemble behavior (Moodie and Passalacqua, 2021).

https://doi.org/10.5194/esurf-2022-66
Preprint. Discussion started: 5 December 2022

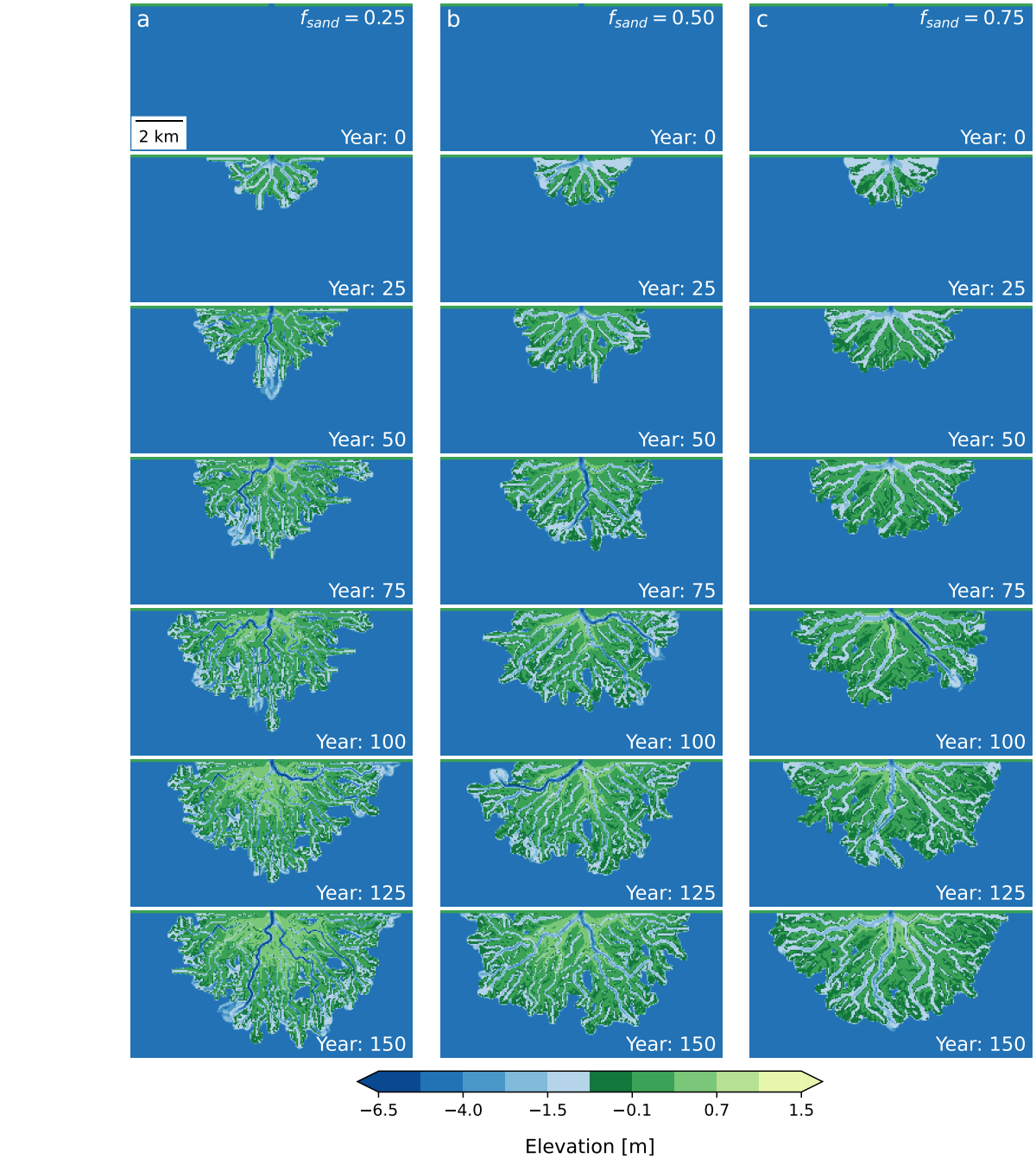

Figure 1. Example timeseries of delta evolution for each of the sand fraction scenarios before any topographic modification: **a:** 25% input sand, **b:** 50% input sand, and **c:** 75% input sand.

https://doi.org/10.5194/esurf-2022-66
Preprint. Discussion started: 5 December 2022


Earth Surface Dynamics Discussions
Open Access
EGU

2.2 Human Modifications to Topography

To capture the influence of human modifications on transport processes within deltaic landscapes, we develop two automated workflows to modify the final `pyDeltaRCM` topography (Figure 2). The first deepens the primary active channel to simulate the dredging of a shipping or navigation channel. The second raises the land of the largest contiguous island on the delta surface to mimic the effect of embanking or poldering a region for human habitation, agriculture, or industrial activities.

2.2.1 Channel Dredging

We identify and artificially deepen the channel conveying the most flow at the end of the `pyDeltaRCM` simulation to simulate dredging. First, we identify the position of the deltaic shoreline using the opening angle method (Shaw et al., 2008) using three ''looks,'' a threshold angle of 75 degrees, and an elevation threshold of 0.5 m below sea level to include the low lying shallow marine environment (Liang et al., 2016b). Next, we morphologically dilate this shoreline twice and intersect it with the array of water discharge values (Figure 2b). Then we identify the location of maximum discharge along the shoreline, and define the minimum cost path (van der Walt et al., 2014) connecting the inlet to this point along a cost array which we define using the discharge array, assigning values of -1 where discharge exceeds 1 m^3/s, and 100 elsewhere (Figure 2c). This routine identifies the largest channel on the delta. We further extend this path 2 km into the receiving basin in the direction of the vector connecting the inlet and the channel outlet previously identified along the shoreline (Figure 2d). We morphologically dilate this single pixel path once to mimic a dredged channel wide enough for shipping, producing a 3 pixel wide (150 m) dredged channel. Then, we lower the topography along the entire channel path to an elevation of -10 m, 5 m below the inlet channel depth, and deeper than natural channels in the delta (Figure 2e). We choose -10 m as our dredged channel depth as this is similar to dredged depths in real navigational channels, such as those in the Western Scheldt estuary (14.5 m, van Dijk et al., 2021) and the Corpus Christi Ship Channel (14.33 m, Valseth et al., 2021). In this simplified dredging scheme we do not account for spoil material.

2.2.2 Island Poldering

We conduct simplified poldering, or embanking, of the largest island in the simulated deltas by raising its elevation to 10 m above sea level. First, we use the previously identified shoreline to delineate the land extents of the delta (Figure 4d). Then, we threshold the water velocity array using a value of 0.3 m/s, the modeled sediment mobility threshold, to identify channelized pixels (Liang et al., 2016b). We perform a morphological closing operation on the array of channelized pixels to connect some of the smaller channel features (Figure 2f). Next, we subtract the array of channelized pixels from the land extents, to isolate the individual islands (Figure 2g). From these individual island objects, we identify the largest by area as the one which will be raised (Figure 2h). We apply a morphological closing operation to this island area to close off any small channels and embayments, and then we perform a morphological erosion operation twice to prevent the poldered landmass from encroaching on adjacent active channels. Finally, we raise the topography in the location of this modified island footprint to an elevation of 10 m, an elevation representative of some of the highest embankments found in real deltas (Wang et al., 2021), well above the

https://doi.org/10.5194/esurf-2022-66
Preprint. Discussion started: 5 December 2022

Earth Surface Dynamics Discussions
Open Access
EGU

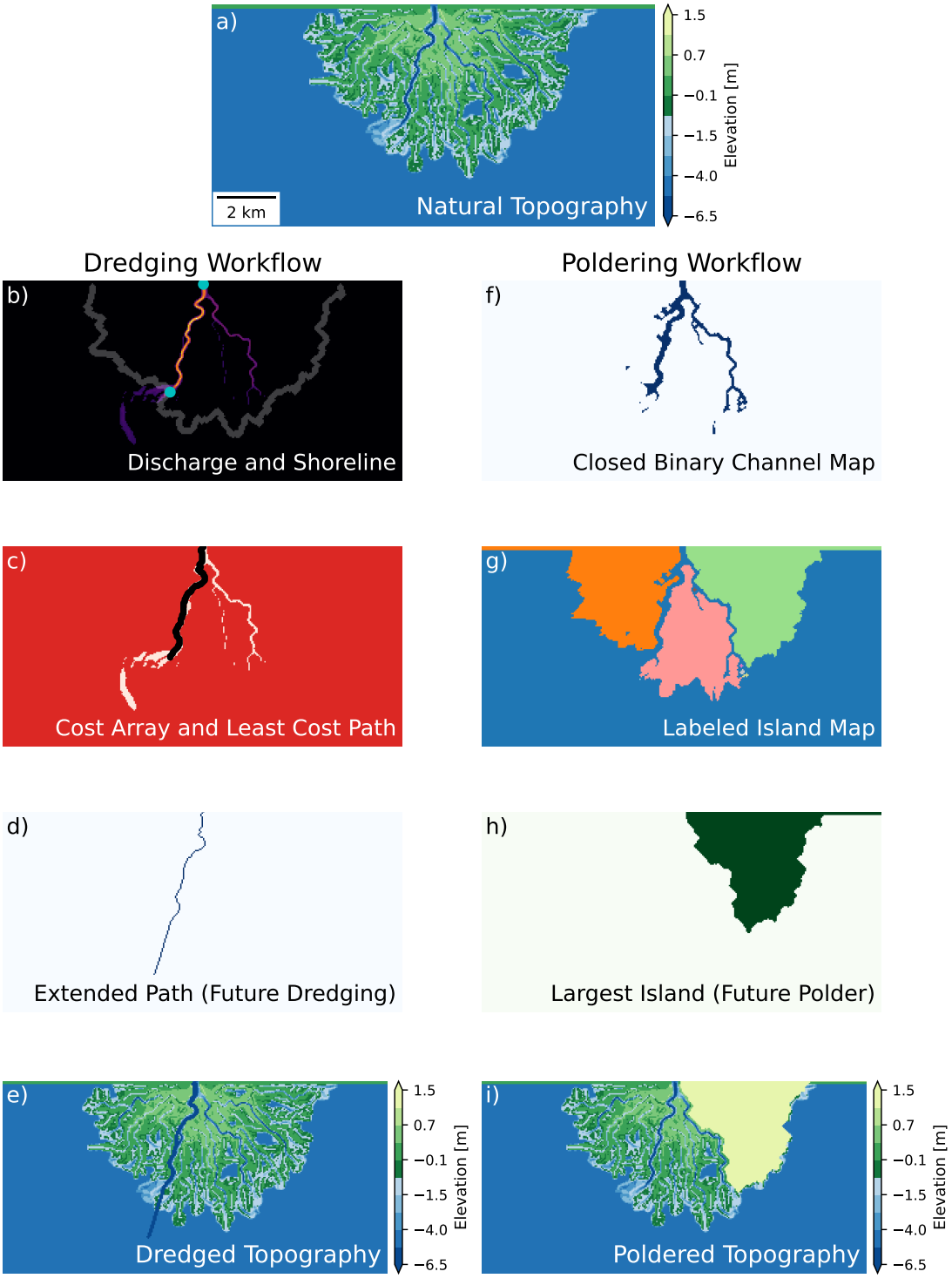

Figure 2. Examples of the two topography modification workflows starting from one final topography (**a**). **b-e:** The dredging workflow. **f-i:** The poldering workflow.

https://doi.org/10.5194/esurf-2022-66
Preprint. Discussion started: 5 December 2022

Earth Surface Dynamics Discussions
Open Access
EGU

sea level of 0 m (Figure 2i). In this simplified poldering scheme we assume the embankment material has been sourced off site. We design our simplified embankments such that they will not be over-topped, a common practice in numerical studies (e.g., Angamuthu et al., 2018); so whether or not the interior is raised does not influence the results.

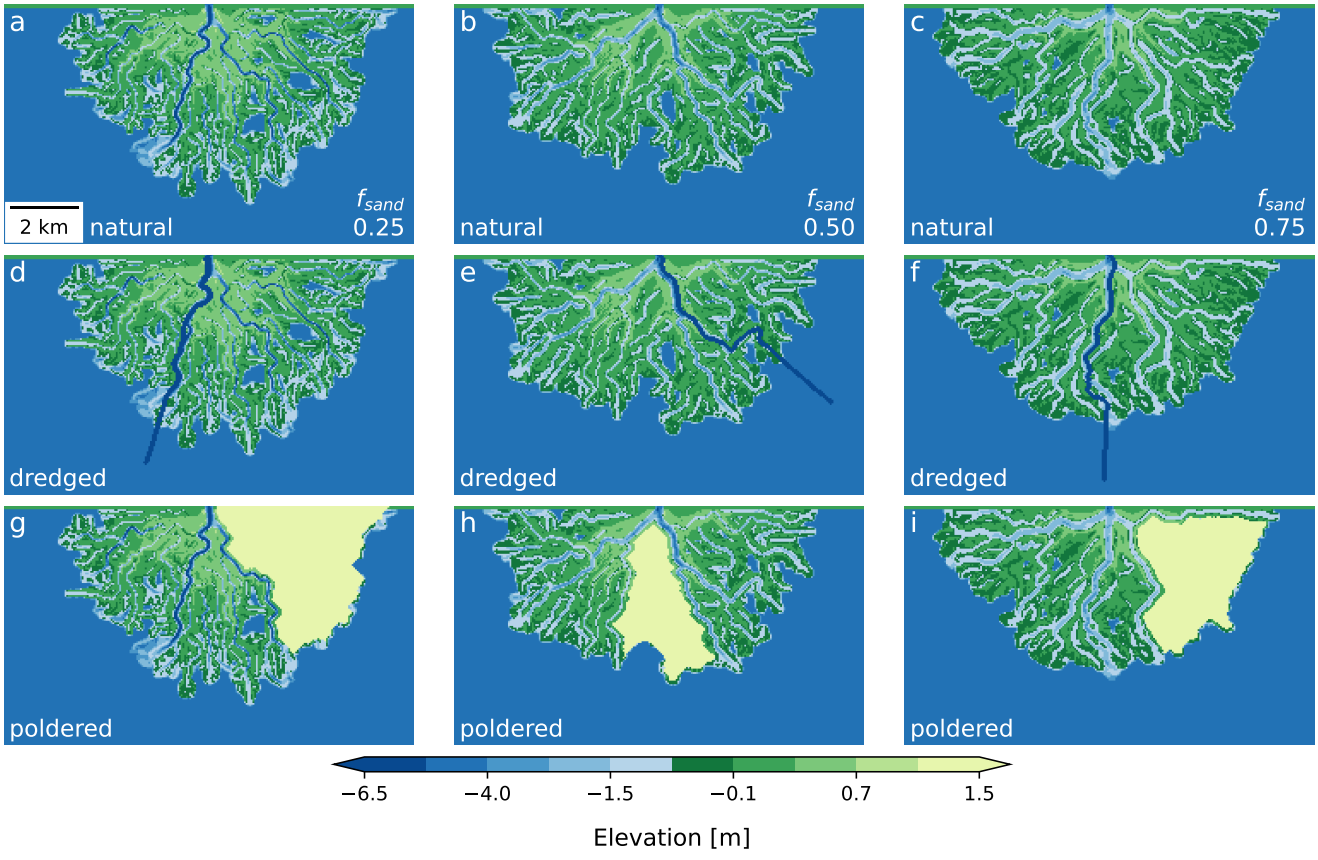

Figure 3. Examples of the different topography modifications. **a, b, c:** ''Natural'' delta topographies with no human modifications. **d, e, f:** ''Dredged'' delta topographies where the dominant channel has been dredged to a depth of 10 m below sea level. **g, h, i:** ''Poldered'' delta topographies where the largest island is identified and raised to an elevation of 10 m above sea level.

2.3 Hydrodynamic Modeling

We simulate sub-annual hydrodynamics using the `ANUGA` model (Nielsen et al., 2005; Roberts et al., 2015). `ANUGA` provides a finite-volume solution to the shallow water equations over an unstructured triangular mesh, enabling the simulation of unsteady and tidal flow conditions which the `pyDeltaRCM` reduced-complexity solution does not provide. We chose the `ANUGA` model because it has been previously used in coastal environments (e.g., Kain et al., 2020; Wright et al., 2022), is fully parallelizable via the Message-Passing Interface (Roberts et al., 2007), and is open-source (Roberts et al., 2015). We define an unstructured

https://doi.org/10.5194/esurf-2022-66
Preprint. Discussion started: 5 December 2022

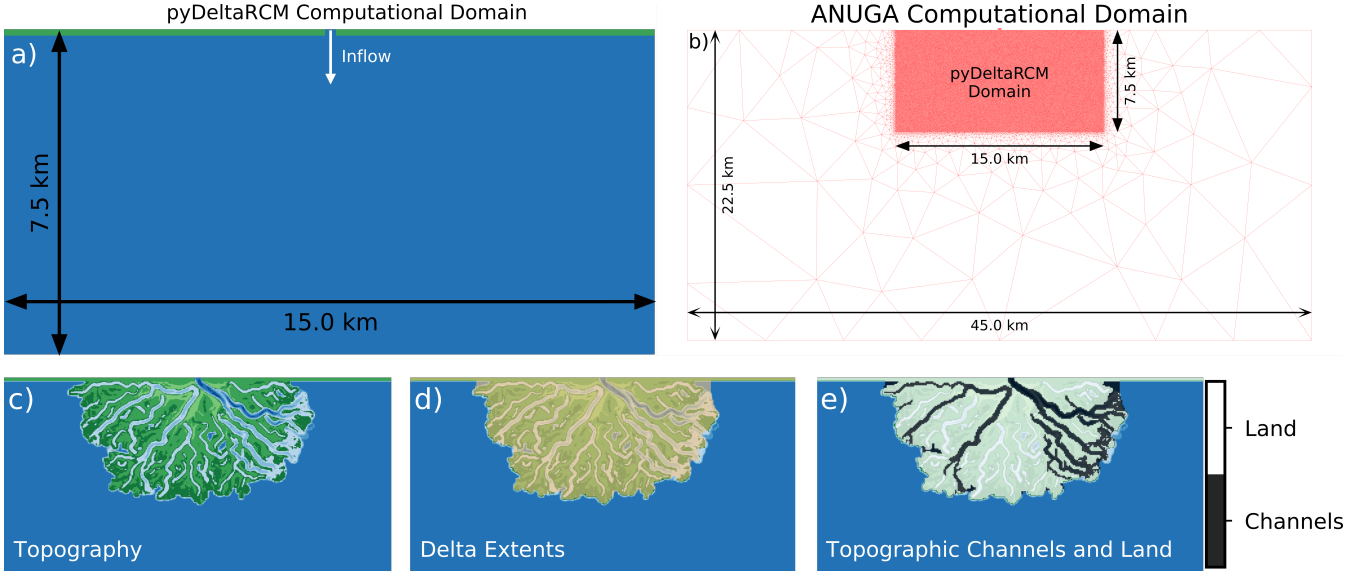

Figure 4. a: The `pyDeltaRCM` computational domain. **b:** The `ANUGA` computational domain. **c:** An example of deltaic topography. **d:** The extracted delta extents for that topography. **e:** The extracted regions of channels and land, defined by topography, within the delta.

mesh with variable cell resolution, such that the high resolution area encompassing the original `pyDeltaRCM` computational domain has a maximum triangle area of 1,250 m^2, which is half the area of a `pyDeltaRCM` cell, to ensure that all topographic features simulated on the regular grid are captured (Figure 4b; see Table A3 for mesh edge length statistics). In the areas of the `ANUGA` computational domain which extend beyond the `pyDeltaRCM` domain, we apply a coarser resolution and set the elevation of the triangles based on the receiving `pyDeltaRCM` basin (-5 m). Within the delta, we apply a k-nearest neighbor interpolation using an inverse-distance weighting to the three nearest neighbors (Maneewongvatana and Mount, 1999; Virtanen et al., 2020) to translate topography values from the `pyDeltaRCM` model grid to the `ANUGA` mesh.

We use the interpolated topography information from `pyDeltaRCM` to initialize the `ANUGA` model for the steady flow simulations. We initialize the domain by filling cells with elevations below sea level (0 m) with water, and then impose a small flow of 0.01 m^3/s in the direction of the inflow channel across the domain to accelerate model convergence to steady-state. Friction in the model is set as a constant Manning's n value of 0.04 across the domain, chosen to strike a balance between the lower values expected in channels and higher values expected in the floodplains (Chow, 1959). In all `ANUGA` simulations we use the second-order temporal resolution numerical solver with the ''low Froude'' setting to reduce flux-damping (Roberts et al., 2015; Wright et al., 2022). For the steady-state simulations we apply the same inlet discharge used in the `pyDeltaRCM` model (1,250 m^3/s) and define the boundary conditions on the top, left, and right sides of the domain as no-flow (reflective) boundaries, and the bottom (bay-side) boundary as a Dirichlet boundary with a fixed water surface elevation of 0 m (Wright et al., 2022). We simulate steady-state bankfull discharge by running the model for 1 day (24 hours) of simulated time using a 15-minute yieldstep, which is the time-interval at which model information is written to the output file. For the unsteady

https://doi.org/10.5194/esurf-2022-66
Preprint. Discussion started: 5 December 2022

tidal simulations we use the final steady-state flow information to initialize the model. At the bottom (bay-side) boundary, we define a semidiurnal tidal signal using a sine wave with an amplitude of 0.25 m, a period of 12 hr, and a mean value of 0 m (sea level) based on numerical models developed for the Wax Lake Delta (Olliver et al., 2020; Wright et al., 2022), a system of similar size and basin properties to our `pyDeltaRCM`-simulated landscapes (Liang et al., 2015, 2016b). We run the unsteady simulations for a total of 24 hours, capturing 2 full tidal cycles, with a yieldstep of 15 minutes, a temporal resolution which has been found to be sufficient for capturing time-varying dynamics in `ANUGA` simulations of both deltas (Wright et al., 2022) and river-floodplain systems (Tull et al., 2022).

2.4 Particle Routing

We transform the unstructured `ANUGA` output data back to a rectilinear grid with 50 x 50 m cells using the same inverse-distance interpolation based on the three nearest neighbors to each grid cell. On the gridded hydrodynamic flow fields, we perform Lagrangian particle routing using the passive particle package `dorado` (Hariharan et al., 2020). `dorado` adapts the DeltaRCM weighted random walk scheme to move passive particles through a flow field while tracking the transport time associated with each individual particle movement, as well as its location. For each ''step'' a particle takes, `dorado` computes its transport time (T_t) using the harmonic average of velocity values taken from the origin (o) and destination (i) locations,

$$T_t = \frac{1}{2} \times d_{eq} \times \left(\frac{1}{v_o} + \frac{1}{v_i} \right) \times (1 + [dc \times U(-0.5, 0.5)]), \tag{1}$$

where d_{eq} is the distance the particle travels along the mean flow path, dc is a diffusivity coefficient (set to the default value of 0.2), and $U(-0.5, 0.5)$ is a uniform distribution centered at 0. For the tidal hydrodynamic simulation results, because our tidal signal is periodic, we loop the final full semidiurnal `ANUGA` output data (hours 12-24) for 7 days to create the set of flow fields over which we route the particles. To ensure that the unsteady particle results are not influenced by the point within the tidal cycle at which they were injected, we inject 250 particles at the apex every 15 minutes over the first full tidal cycle (Wright et al.), for a total of 12,000 particles. We match this process for the steady hydrodynamic simulation results, except we use the final `ANUGA` flow information (Figure A1), as the flow fields are unchanging in time. In both the steady and unsteady cases, we route the particles through the domain for the remainder of the 7 days at a 15 minute increment, matching the yieldstep of the `ANUGA` simulation results (Figures A2 & A3).

We configure `dorado` to consider cells with water depths below 1 cm to be impassable to particles, and define the `dorado` dispersion parameter (γ) using the default value of 0.05 (Liang et al., 2015; Hariharan et al., 2020; Tull et al., 2022). In `dorado`, the weighted random walk taken by the particles involves a combination of the water surface slope and discharge to determine the downstream direction from any given point, F^* (Liang et al., 2015; Hariharan et al., 2020). Using this downstream direction, the weight for adjacent cell i, is computed as

$$w_i = \frac{h_i^{\theta} \max(0, F^* \cdot d_i)}{\Delta_i}, \tag{2}$$

where d_i is the downstream unit vector, Δ_i is the distance downstream, and h_i is the water depth of the downstream cell and is raised to the user-defined parameter θ (Liang et al., 2015; Hariharan et al., 2020). In the DeltaRCM framework, this θ parameter

https://doi.org/10.5194/esurf-2022-66
Preprint. Discussion started: 5 December 2022

is varied to mimic the behavior of different sediments, as it controls the dependence the random walk weights have on water depth. Wright et al. suggest that θ can be varied to simulate the transport behavior of different material types. For example, positively-buoyant material would be modeled using $\theta < 1$, while negatively-buoyant material would use $\theta > 1$ (Wright et al.). In this work we select three θ values, 0, 1, and 2, to simulate the movement of positively, neutrally, and negatively buoyant material respectively (Figure A4).

2.5 Topographic Delineation of Channels and Islands

To quantify particle behavior within different regions of the broader landscape, we divide the delta into active channels and islands (land) based on topography. We elect to threshold the individual models by topography rather than any aspects of the flow behavior, as the anthropogenic modifications alter the flow through the landscape, potentially confounding any particle results calculated using flow-based delineations. To quantify the bulk behavior of particles within the delta channels and islands, we threshold the topography at an elevation of -0.5 m (after Liang et al., 2016b; Lauzon and Murray, 2018), and identify the largest contiguous set of cells with elevations below -0.5 m. We define those cells as the combination of the channel network and the ocean cells, and mask them using the delta extents (Figure 4d), to determine the topographic channel area within the delta (Figure 4e). Next we invert this map of the topographic channels to identify the delta islands (Figure 4e). Using these two classes it becomes possible to disentangle particle behavior within the delta landscape to distinguish between the behavior of particles within channels and those within islands, which is important to understand as significantly greater amounts of biogeochemical processing occur within deltaic islands than channels (e.g., Hiatt et al., 2018; Knights et al., 2020).

2.6 Nourishment Areas

We apply the idea of nourishment areas for distributary networks (Edmonds et al., 2011) to capture the area of the delta surface visited by the passive particles. In addition to capturing the locations visited by particles, we quantify the normalized visit frequency for every location within the delta (Figure 5; Wright et al.). For all nourishment area metrics, we clip the particle paths to the land extents of the delta (as defined in Section 2.2.2; Figure 4d).

2.7 Exposure Times

We calculate exposure times for individual particles within a defined area by summing the amount of time a particle spends within that region. A particle's individual exposure time reflects the total amount of time the particle spends within the defined area of interest, even if the particle enters and exits the region multiple times over the course of its travel (Hiatt et al., 2018). Using this methodology, we define exposure time distributions for groups of particles across all modeled scenarios for the different hydrodynamic scenarios simulated (Section 2.3) to compare the influence that sediment composition, flow conditions, and topographic modifications have on the transport of different kinds of material. While we do not explicitly consider any particular nutrients or chemicals in this study, exposure times are commonly used to estimate nutrient removal and other eco-

https://doi.org/10.5194/esurf-2022-66
Preprint. Discussion started: 5 December 2022

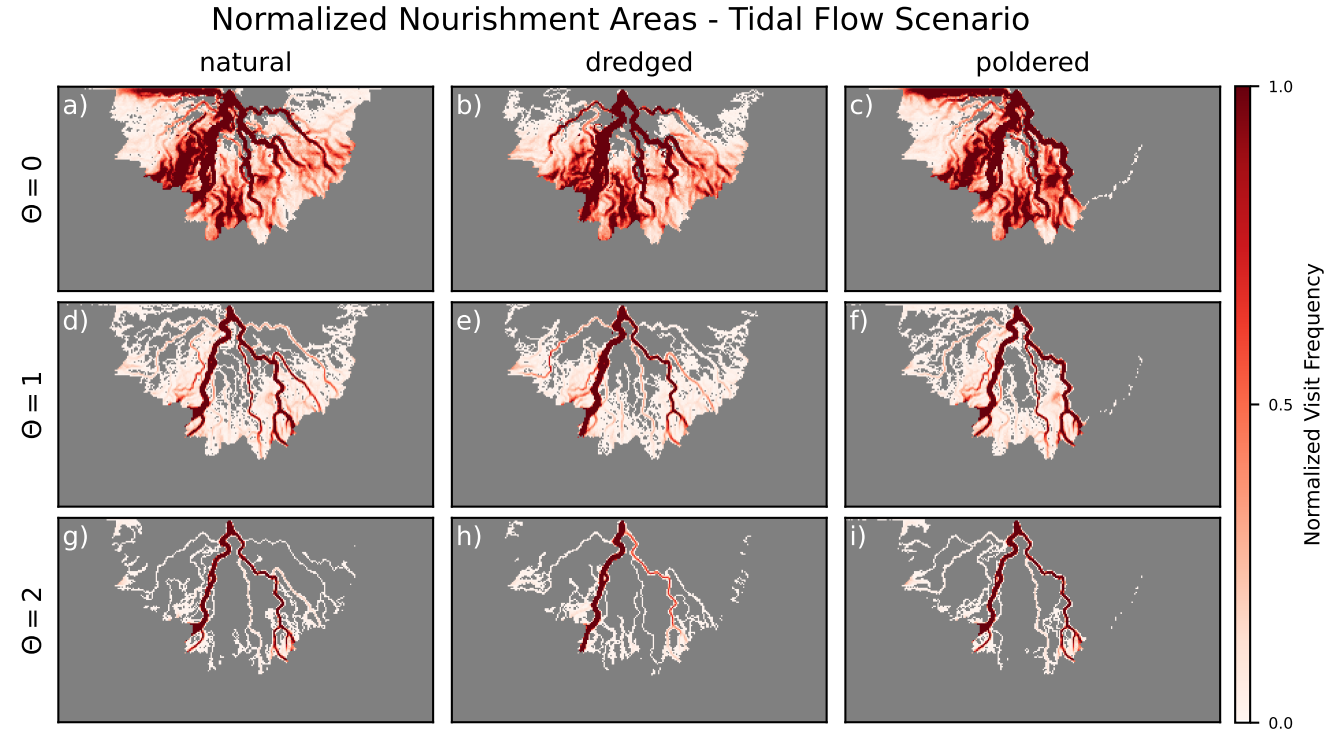

Figure 5. Examples of normalized nourishment frequencies for particles routed for 7 days in the tidal scenario over the topographies shown in Fig. 3a, d, g ($f_{sand} = 0.25$) with different θ parameters to simulate the transport of material through different locations of the water column.

geomorphic processing taking place within the landscape (e.g., de Brauwere et al., 2011; Viero and Defina, 2016; Hiatt et al., 2018).

3 Results

3.1 Area Nourished

We find that the θ parameter, conceptually linked to the vertical position within the water column of the material being transported, has a significant impact on the deltaic area nourished by particles. When $\theta = 0$ (positively-buoyant material), the majority of the wetted delta surface is visited by particles (Figure 5a-c). Conversely, when $\theta = 2$ (negatively-buoyant material), the particles stay predominantly within the larger channels of the system (Figure 5g-i). The first-order differences in transport behavior associated with the type of material, and its dependence on water depth for transport, can be seen across deltas formed by different input sediment loads, and those with different topographic modifications (Figure 6).

https://doi.org/10.5194/esurf-2022-66
Preprint. Discussion started: 5 December 2022

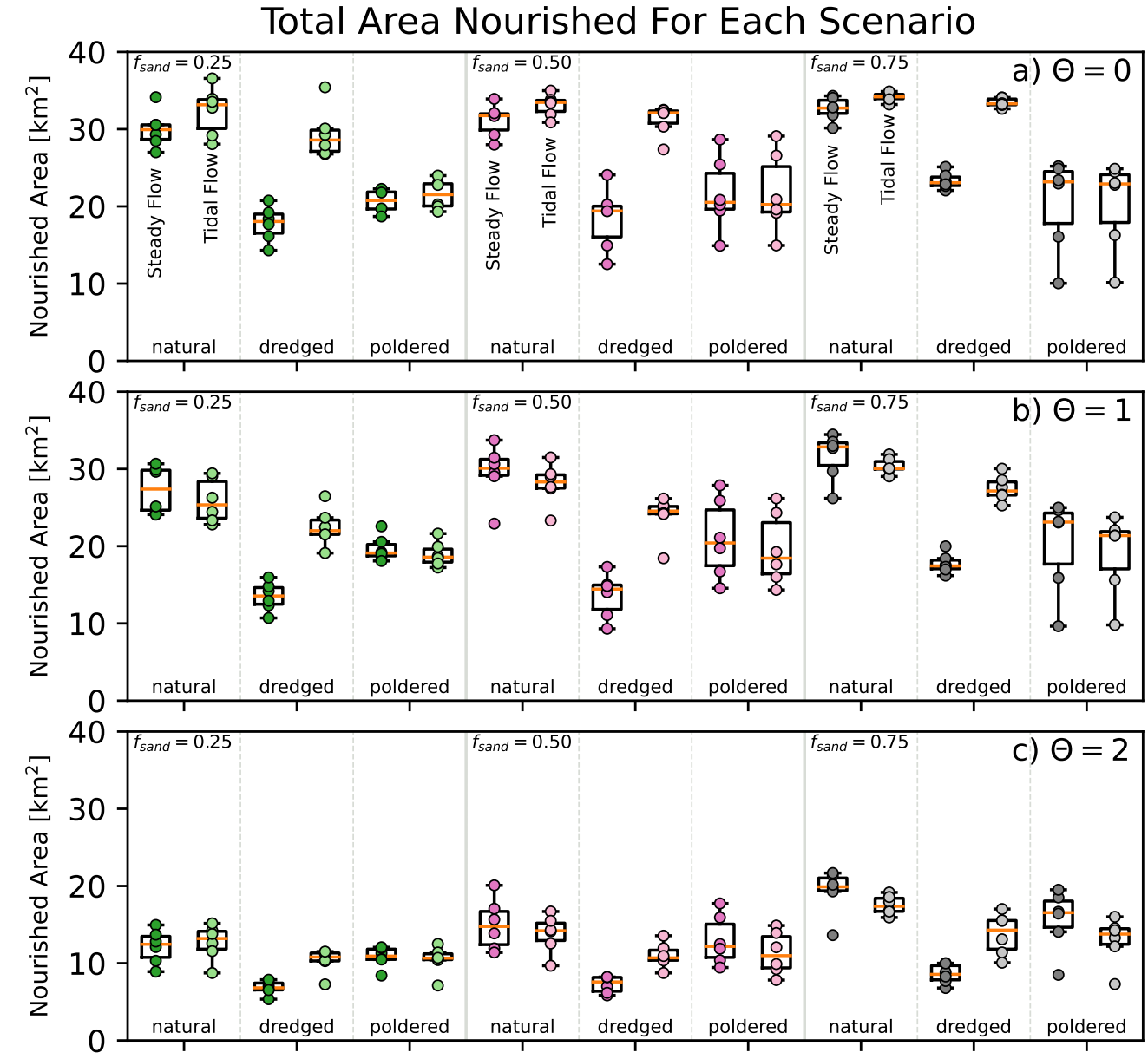

Figure 6. Total area nourished (visited) by particles for each scenario. Individual model replicate results shown as points overlaid on box-plots of the same data. Data are identified by input sand fraction, flow regime, and topographic modification, and further organized on separate axes by the θ parameter with **a)** $\theta = 0$, **b)** $\theta = 1$, and **c)** $\theta = 2$. For select individual particle paths see Fig. A5 & Fig. A6.

https://doi.org/10.5194/esurf-2022-66
Preprint. Discussion started: 5 December 2022

The flow regime has minimal influence on the total area nourished by particles for most scenarios. In the event of channel dredging, however, there is consistently a difference in the nourishment area between the steady and tidal flow simulations across all sediment compositions and particle material types (Figure 6). When the channel is dredged, the presence of tides markedly increases the area of the delta that is visited by particles.

Human modification of delta topography reduces the area visited by particles in both the cases of channel dredging and island poldering (Figure 6). There is greater variability in the nourishment area of poldered topographies, consistent with greater variability in polder areas than dredged channel areas (Tables A1 & A2); we do not normalize our results based on the area of the embanked island or dredged channel.

The input sediment composition responsible for forming deltas also impacts the area nourished. Sediment composition is known to influence the morphology of natural deltas (e.g., Caldwell and Edmonds, 2014; Liang et al., 2016b; Lauzon and Murray, 2018; Hariharan et al., 2021). These morphological differences translate into differences in nourishment area, with the sandier deltas, known to have shallower channels (Liang et al., 2016b), having greater nourishment areas than the muddier systems (Figure 6).

3.2 Timeseries of Island Visitation

The fraction of particles within deltaic islands reveals an early pulse of island occupancy as particles are introduced to the system (hours 0-12) followed by a decay for all materials and scenarios as particles exit the delta and enter the ocean (Figure 7). Material type (θ) exerts a greater control over the fraction of particles within islands than the flow regime or topographic modification across all times and all scenarios (Figure 7). Behavior between the natural and poldered topographies is similar across the different material and flow cases, however the proportion of particles within islands is most reduced for the dredged topographies (Figure 7). The tidal cases show the effect of tides either pushing particles upstream, or accelerating their transport downstream, based on the time. The tidal signal itself is visible in the timeseries plots when $\theta = 0$ (positively-buoyant material). The sand fraction responsible for creating the underlying topography exerts some control over the overall fraction of particles able to visit the islands (Figure 6), and this is further apparent in the timeseries plots as higher peaks (Figure 7).

3.3 Exposure Time Distributions

We plot the cumulative distribution functions for particle exposure times (Figure 8) calculated over the full delta extents (e.g., Figure 4d). To the first-order, exposure times are controlled by the type of material being transported, with positively-buoyant material ($\theta = 0$) spending more time within the delta than negatively-buoyant material ($\theta = 2$, Figure 8). Across all material types the exposure times appear to be longer for muddier landscapes. Dredging lengthens exposure times, while poldering shortens them relative to the distributions associated with natural systems for all θ parameter values considered. When θ is zero (positively-buoyant), tidal flow conditions visibly lengthen exposure times of particles, while this trend is both less consistent, and less visible, for higher values of θ (less buoyant material).

When exposure time distributions are calculated within the topographically delineated channel and island regions (e.g., Figure 4e), the results are varied (Figure 9). For θ values of 1 (neutrally-buoyant) and 2 (negatively-buoyant), exposure times

https://doi.org/10.5194/esurf-2022-66
Preprint. Discussion started: 5 December 2022

Earth Surface Dynamics Discussions
Open Access
EGU

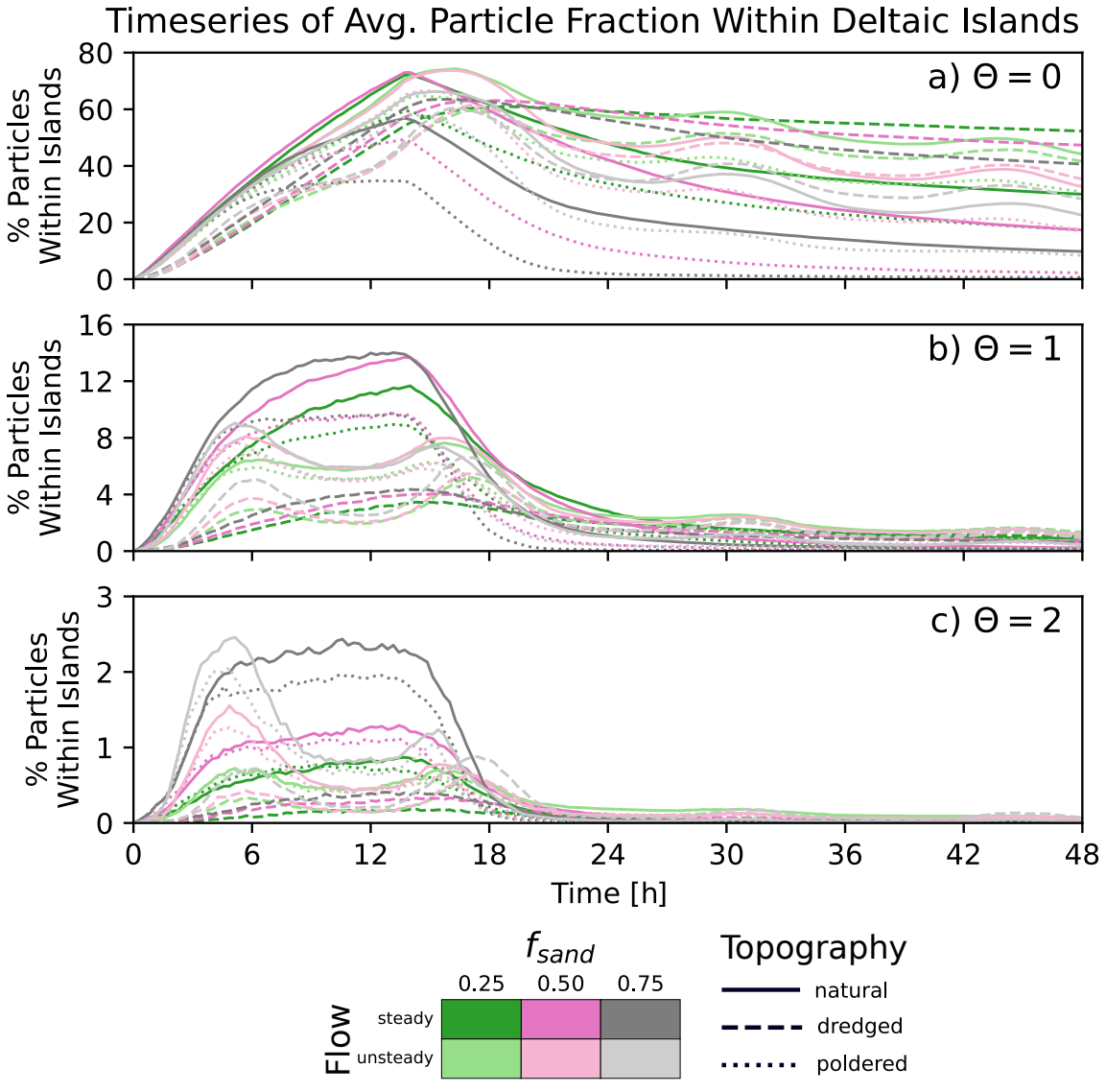

Figure 7. Timeseries of the average percentage of particles to be within deltaic islands for the first 48 hours over which the particles are routed for each modeled scenario. Data is grouped by θ value, with **a)** $\theta = 0$, **b)** $\theta = 1$, and **c)** $\theta = 2$. *Note:* Individual plots have different y-axis limits.

https://doi.org/10.5194/esurf-2022-66
Preprint. Discussion started: 5 December 2022

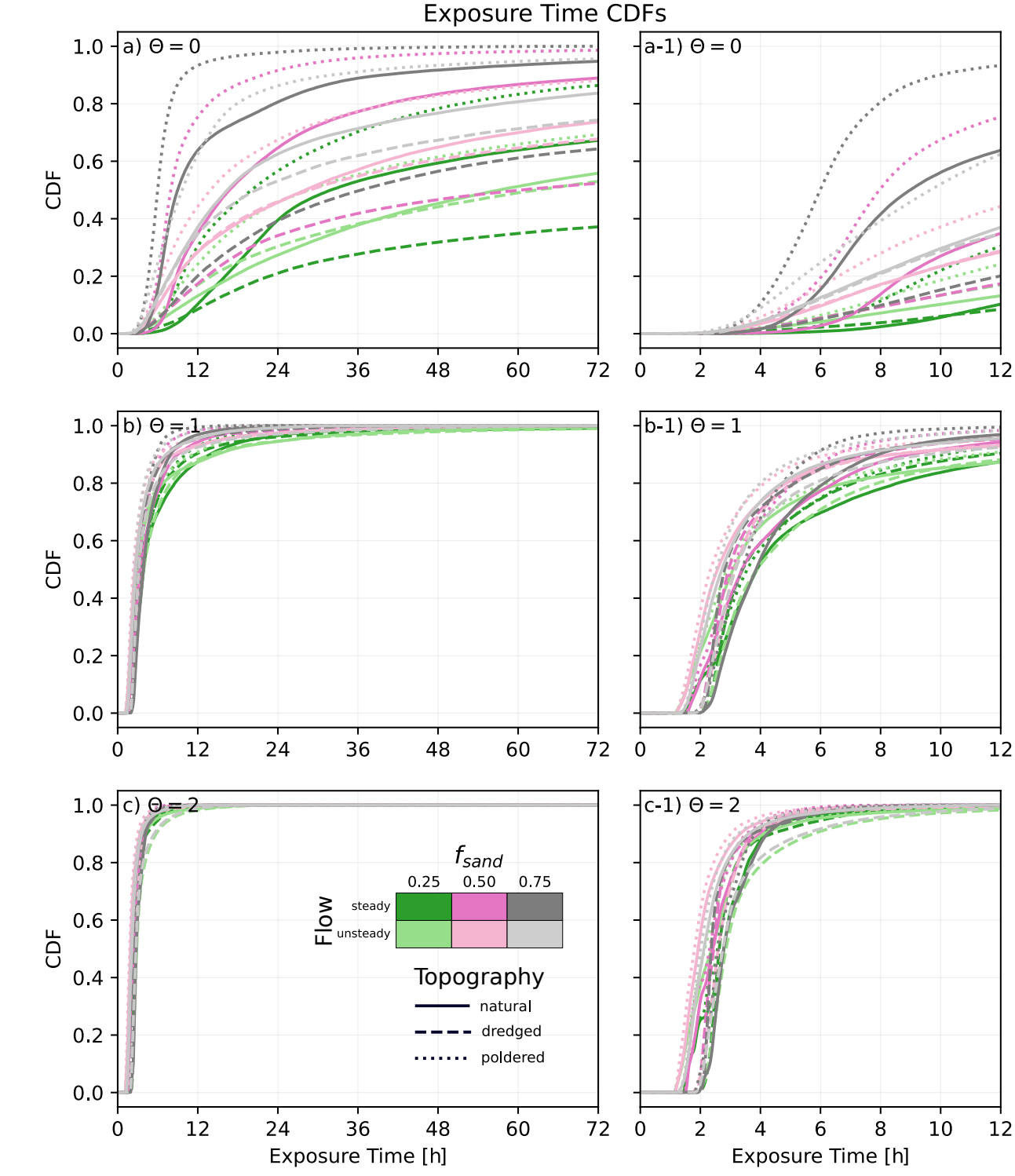

Figure 8. Exposure time cumulative distribution functions (CDFs) for the different scenarios. Data is grouped by θ value, with **a)** $\theta = 0$, **b)** $\theta = 1$, and **c)** $\theta = 2$, with the **a-1, b-1, c-1** designations for zoomed in plots of the same data.

https://doi.org/10.5194/esurf-2022-66
Preprint. Discussion started: 5 December 2022

for particles within channels (Figure 9c, e) are similar to the overall exposure times of particles across the entire delta extents (Figure 8b, c), which is to be expected given the relatively small fraction of particles that enter the deltaic islands (Figure 7b, c). Exposure times for $\theta = 0$ (positively-buoyant) particles within channels (Figure 9a) are shorter compared to those computed across the full delta areas (Figure 8a), as a majority of those particles enter the delta islands (Figure 7a). For exposure times computed within the islands, the results for $\theta = 0$ (Figure 9b) are similar to the overall exposure times (Figure 8a), while the exposure times computed for θ values of 1 and 2 within islands (Figure 9d, f) are shorter than those computed for the channels (Figure 9c, e) or the entire delta extents (Figure 8b, c).

4 Discussion

4.1 Natural Variability

We find that there are differences in material transport behavior solely due to differences in the input sediment composition responsible for forming the landscapes. This is true for both the total area visited by particles (Figure 6) as well as the amount of time particles spend within the delta itself (Figure 8). The finding that sandier deltas tend to have greater nourishment areas (Figure 6) is consistent with studies that have found sandy deltas to have a greater number of channels than muddy systems (Caldwell and Edmonds, 2014; Liang et al., 2016a; Hariharan et al., 2021). When channels are the primary conduit for material transport, it follows logically that a greater number and areal proportion of channels should translate to a higher nourishment area. Exposure time distributions, which reveal that sandier deltas have shorter exposure times than muddier systems (Figure 8), suggest that the presence of a greater number of channels enable the more rapid distribution of material offshore. This finding is also consistent with prior work, which has established that higher mud content (higher sediment cohesion) leads to greater channel sinuosity (Geleynse et al., 2011; Liang et al., 2016b) and higher values of shoreline roughness (Edmonds and Slingerland, 2010; Straub et al., 2015), increasing the length along a channel from the apex to the shoreline. When the distance particles travel from the apex to the shoreline is increased, it is likely they will take a longer time to travel to the ocean than if a shorter path were available.

4.2 Impact of Human Modifications on Transport

Human modifications appear to reduce the connectivity between channels and islands within deltas (Figures 6 & 7). Both channel dredging and island poldering reduce the total area nourished by particles under both steady and tidal flow conditions (Figure 6). This reduction in connectivity is consistent with other studies on modified landscapes (e.g., Angamuthu et al., 2018; van Dijk et al., 2021) and should be expected when projects which significantly modify deltaic topography are undertaken. In coastal environments, altering the topography can change the distribution of salinity in the system leading to adverse ecological impacts (e.g., Ohimain, 1996; Durand, 2017; Wilson et al., 2017). While we do not model salinity directly in this work, we do simulate the transport of material from the apex of the delta, a location at which the water flowing into the system can be assumed to be fresh-water. Consequently, we can conceptualize our particles as fresh-water tracers that move where we would

https://doi.org/10.5194/esurf-2022-66
Preprint. Discussion started: 5 December 2022

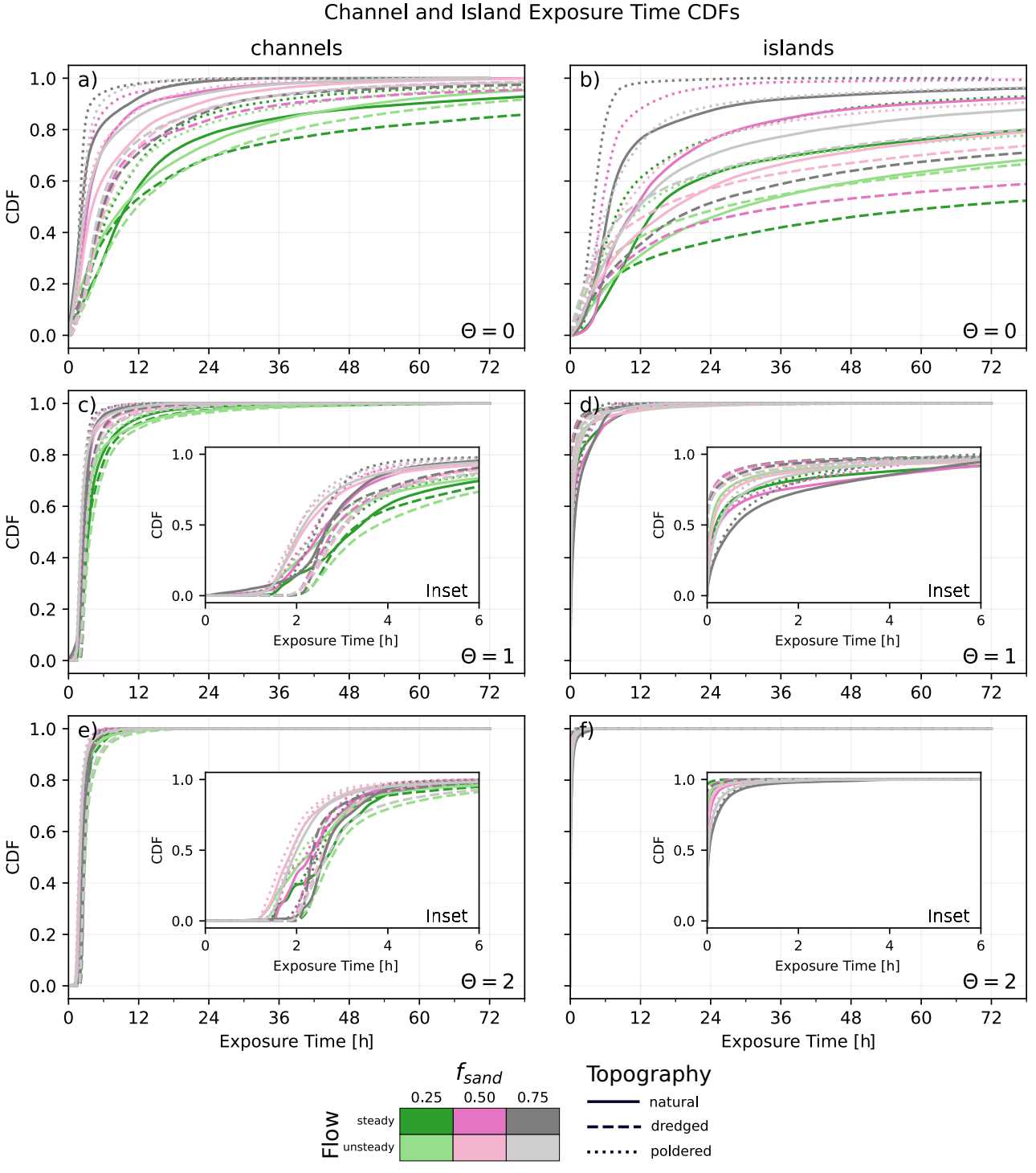

Figure 9. Exposure time cumulative distribution functions (CDFs) for the delta channels and islands (columns). Each row contains results from a different θ value, with **a-b:** $\theta = 0$, **c-d:** $\theta = 1$, and **e-f:** $\theta = 2$. Inset plots focused on exposure time CDFs between 0-6 hours shown for **c-f**.

https://doi.org/10.5194/esurf-2022-66
Preprint. Discussion started: 5 December 2022

expect the river water to flow. With this in mind, the timeseries of particle visitation to islands (Figure 7) may be indicative of the relative flux of fresh-water into these landscape elements. The island exposure times (Figure 9b, d, f) more directly provide a measure of the expected water age for the islands, and how it may change as a result of human modifications to the topography. The exposure of particles to islands may be of particular importance for biogeochemical processing occurring on the delta (e.g., Hiatt et al., 2018; Knights et al., 2020; Christensen et al., 2020).

Our finding that exposure times within islands are shorter than those within channels is a counter-intuitive result (Figure 9), for which one possible explanation is related to the topographic delineation of channels and islands (Figure 4e). While topographic lows within islands are still defined as part of the island, the definition of the channels using the largest contiguous area below -0.5 m (Section 2.5) results in a number of relic channels near the shoreline being counted as channels in our exposure time analysis (Figure 4e). Given that the channels become shallower near the coastline, and the tides re-circulate particles near the coast in the tidal scenarios, this may be the reason the particle exposure times appear to be longer in the channels than in the islands. Another potential explanation is that particles may take short incursions onto the island pixels for only one or two timesteps, limiting their exposure to the island areas, and staying within fast moving flows. The overarching pattern of exposure times with respect to the material type (θ value), however, matches our findings for the exposure times computed over the entire delta extents (Figure 8), with higher θ values (less-buoyant material) having shorter exposure times.

4.3 Transport Differences Due to Material Properties

Despite adopting a reduced-complexity approach for simulating the transport of different materials, we see marked differences in their transport behavior (Figures 5, 6, 7, 8). Material buoyancy has a greater impact on both nourishment area (Figure 6) and exposure time (Figure 8) than the flow regime, or any modifications made to the topography. This result highlights the importance of simulating attributes of the material(s) of interest when performing a more detailed site or case-specific study. Interestingly, the relative transport behavior between different flow conditions and topographies does not necessarily transfer across different material types. For example, particles on the poldered topographies with $\theta = 0$ (positively-buoyant) appear to spend the least amount of time in the channels and islands, however, it is the dredged topographies that have the shortest exposure times in the islands when the θ parameter is 1 (neutrally-buoyant) or 2 (negatively-buoyant, Figure 9).

4.4 Study Limitations and Implications for Future Studies

As we adopted a reduced-complexity numerical modeling approach to this study, we were able to isolate the effects of sediment composition, topographic modifications, flow conditions, and material type on transport through deltaic environments. While this exploratory approach is informative, there are a number of limitations associated with the methods we chose to employ. The `pyDeltaRCM` morphodynamic model, used to create the delta landscapes, is capable of producing realistic river-dominated delta landforms (Liang et al., 2016b), but there are a number of other forcings which shape delta morphology that we do not account for, such as waves, vegetation, wind, variable discharge, ice, subsidence, and other environmental factors (e.g., Galloway, 1975; Sassi et al., 2012; Anthony, 2015; Piliouras et al., 2017; Lauzon and Murray, 2018; Zoccarato et al., 2018; Chamberlain et al., 2021). Furthermore, our simplified approach to modifying the topography to reflect channel dredging and

https://doi.org/10.5194/esurf-2022-66
Preprint. Discussion started: 5 December 2022

island embanking does not account for the sourcing or dumping of the material used to make those changes. In the case of channel dredging, for example, it is common to use the adjacent land as the spoil location for dredge material (e.g., Mossa and Chen, 2021).

These types of local morphological changes can alter the hydrodynamics and morphodynamics of the system (Wilson et al., 2017; Bain et al., 2019). In this work we do not conduct any morphodynamic modeling after modifying the topography, although we know that sediment transport continues to occur, often infilling channels (Wilson et al., 2017). When we simulate short-term hydrodynamics, we move to a more complex model by using `ANUGA` to resolve the shallow-water equations over our domain, however in doing so, we explicitly do not consider vertical flow behavior, and are limited by the spatial resolution of our mesh. When we vary the θ parameter for the `dorado` simulations, we are adding a reduced-complexity representation of vertical sorting back into our simulation (Wright et al.), but this is not as rigorous as a full 3-D flow and particle tracking approach (e.g., Dagestad et al., 2018). However, limited data often prevents 3-D hydrodynamic models from being more accurate than 2-D solutions (Bates, 2022).

Despite these limitations, we believe the results presented here have important implications for future studies. The delta landscapes simulated are generated over 150 years of simulated time and are similar in scale to the Wax Lake Delta (Liang et al., 2015, 2016b). Consequently, these findings can inform future river diversion and land building projects and complement prior studies done on connectivity and material transport in similar environments (e.g., Hiatt and Passalacqua, 2015; Sendrowski and Passalacqua, 2017; Hiatt et al., 2018; Esposito et al., 2020). Uniquely, numerical models of delta landscapes provide us with a degree of control over input sediment characteristics, flow scenarios, and topographic modifications, unachievable for studies conducted on real landscapes. We find that maps of particle nourishment (e.g., Figure 5) are qualitatively similar to numerical results, tracer studies, and remotely sensed streaklines, presented in studies of specific deltas (Shaw et al., 2016; Hiatt et al., 2018; Wright et al.).

From these results, we establish that flow conditions and topography exert large influences over the transport and behavior of material traveling near the top of the water column (Figures 5a-c, 8a, 9). Conversely, if the primary material of interest travels low in the water column, then perhaps there may be less of a need to conduct rigorous analysis of the impact dredging or embankment construction will have on transport, as the majority of material remains within the channels (Figure 5g-i, 6c, 9). Furthermore, by testing these different flow regimes and topographic modifications on different natural topographies, we show that the antecedent conditions also influence the connectivity of a landscape, and topographic modifications can alter that connectivity. These results present approximate magnitudes of expected changes to transport behavior for a number of scenarios, and may help delta managers prior to commissioning a detailed study on the effects of proposed modifications.

5 Conclusions

In this work we provide a comprehensive look at the influence of natural topography, channel dredging, island embankment, and flow conditions on the transport of material through river deltas. To do this, we applied a series of three numerical models,

https://doi.org/10.5194/esurf-2022-66
Preprint. Discussion started: 5 December 2022

pyDeltaRCM, ANUGA, and dorado to simulate a deltaic landscape, model hydrodynamic flow fields, and route passive Lagrangian particles, respectively. We found that:

- Properties of the material itself (simulated here by varying the θ parameter) act as a first order control on the total area nourished by particles and their exposure time distributions
- Human modifications to delta topography reduce the area nourished by passive particles
- The construction of polders reduces the exposure times of particles within the delta, while the dredging of channels increases exposure times relative to exposure times calculated over the natural topography.

We qualitatively find the overall patterns of nourishment behavior to be quite similar to results from site-specific studies (Wright et al.), supporting our belief that these exploratory results can be applied to inform and guide future studies on material transport through coastal deltas.

Code and data availability. Models used in this work are all open-source and freely available. pyDeltaRCM (Moodie et al., 2021) is available at: https://github.com/DeltaRCM/pyDeltaRCM; ANUGA (Nielsen et al., 2005; Roberts et al., 2015) is available at: https://github.com/GeoscienceAustralia/anuga_core; and dorado (Hariharan et al., 2020) is available at: https://github.com/passaH2O/dorado.

Author contributions. JH and PP designed and conceived of the research project. JH and AM developed the pyDeltaRCM modeling approach. JH, KW, and NT developed the ANUGA modeling approach. All authors designed and developed the dorado particle routing methods. JH performed the analysis and wrote the first draft. All authors reviewed and edited the original draft.

Competing interests. The authors have the following competing interests: At least one of the (co-)authors is a member of the editorial board of Earth Surface Dynamics.

Acknowledgements. The authors acknowledge support from the National Science Foundation via EAR-1719670 and EAR-1952772, the NSF GRFP under DGE-1610403, the NASA Delta-X project which is funded by the Science Mission Directorate's Earth Science Division through the Earth Venture Suborbital-3 Program NNH17ZDA001N-EVS3, and the Graduate School at the University of Texas.

Video supplement. Videos of pyDeltaRCM model evolution, as well as dorado particle results for both the steady and unsteady cases are available via the Open Science Framework (OSF) at: https://doi.org/10.17605/OSF.IO/D95ZN.

https://doi.org/10.5194/esurf-2022-66
Preprint. Discussion started: 5 December 2022

References

Al Masud, M. M., Gain, A. K., and Azad, A. K.: Tidal river management for sustainable agriculture in the Ganges-Brahmaputra delta: Implication for land use policy, Land Use Policy, 92, 104 443, https://doi.org/10.1016/j.landusepol.2019.104443, 2020.

Angamuthu, B., Darby, S. E., and Nicholls, R. J.: Impacts of natural and human drivers on the multi-decadal morphological evolution of tidally-influenced deltas, Proceedings of the Royal Society A: Mathematical, Physical and Engineering Sciences, 474, 20180 396, https://doi.org/10.1098/rspa.2018.0396, 2018.

Anthony, E. J.: Wave influence in the construction, shaping and destruction of river deltas: A review, https://doi.org/10.1016/j.margeo.2014.12.004, 2015.

Auerbach, L. W., Goodbred Jr, S. L., Mondal, D. R., Wilson, C. A., Ahmed, K. R., Roy, K., Steckler, M. S., Small, C., Gilligan, J. M., and Ackerly, B. A.: Flood risk of natural and embanked landscapes on the Ganges–Brahmaputra tidal delta plain, Nature Climate Change, 5, 153–157, https://doi.org/10.1038/nclimate2472, 2015.

Bain, R. L., Hale, R. P., and Goodbred, S. L.: Flow Reorganization in an Anthropogenically Modified Tidal Channel Network: An Example From the Southwestern Ganges-Brahmaputra-Meghna Delta, Journal of Geophysical Research: Earth Surface, 124, 2141–2159, https://doi.org/10.1029/2018JF004996, 2019.

Banas, N. S., MacCready, P., and Hickey, B. M.: The Columbia River plume as cross-shelf exporter and along-coast barrier, Continental Shelf Research, 29, 292–301, https://doi.org/10.1016/j.csr.2008.03.011, 2009.

Bates, P. D.: Flood Inundation Prediction, Annual Review of Fluid Mechanics, 54, 287–315, https://doi.org/10.1146/annurev-fluid-030121-113138, 2022.

Cai, H., Savenije, H. H. G., Yang, Q., Ou, S., and Lei, Y.: Influence of River Discharge and Dredging on Tidal Wave Propagation: Modaomen Estuary Case, Journal of Hydraulic Engineering, 138, 885–896, https://doi.org/10.1061/(asce)hy.1943-7900.0000594, 2012.

Caldwell, R. L. and Edmonds, D. A.: The effects of sediment properties on deltaic processes and morphologies: A numerical modeling study, Journal of Geophysical Research: Earth Surface, 119, 961–982, https://doi.org/10.1002/2013JF002965, 2014.

Chamberlain, E. L., Shen, Z., Kim, W., McKinley, S., Anderson, S., and Törnqvist, T. E.: Does Load-Induced Shallow Subsidence Inhibit Delta Growth?, Journal of Geophysical Research: Earth Surface, 126, e2021JF006 153, https://doi.org/10.1029/2021JF006153, 2021.

Chow, V. T.: Open-channel hydraulics, McGraw-Hill civil engineering series, 1959.

Christensen, A., Twilley, R. R., Willson, C. S., and Castañeda-Moya, E.: Simulating hydrological connectivity and water age within a coastal deltaic floodplain of the Mississippi River Delta, Estuarine, Coastal and Shelf Science, 245, 106 995, https://doi.org/10.1016/j.ecss.2020.106995, 2020.

Dagestad, K. F., Röhrs, J., Breivik, O., and Ådlandsvik, B.: OpenDrift v1.0: A generic framework for trajectory modelling, Geoscientific Model Development, 11, 1405–1420, https://doi.org/10.5194/gmd-11-1405-2018, 2018.

Day, J. W., Britsch, L. D., Hawes, S. R., Shaffer, G. P., Reed, D. J., and Cahoon, D.: Pattern and process of land loss in the Mississippi Delta: A spatial and temporal analysis of wetland habitat change, Estuaries, 23, 425–438, https://doi.org/10.2307/1353136, 2000.

Day, J. W., Gunn, J. D., Folan, W. J., Yáñez-Arancibia, A., and Horton, B. P.: Emergence of complex societies after sea level stabilized, Eos, 88, 169–170, https://doi.org/10.1029/2007EO150001, 2007.

de Brauwere, A., de Brye, B., Blaise, S., and Deleersnijder, E.: Residence time, exposure time and connectivity in the Scheldt Estuary, Journal of Marine Systems, 84, 85–95, https://doi.org/10.1016/j.jmarsys.2010.10.001, 2011.

https://doi.org/10.5194/esurf-2022-66
Preprint. Discussion started: 5 December 2022

Durand, J. R.: Evaluating the aquatic habitat potential of flooded polders in the Sacramento-San Joaquin Delta, San Francisco Estuary and Watershed Science, 15, https://doi.org/10.15447/sfews.2017v15iss4art4, 2017.

Edmonds, D. A. and Slingerland, R. L.: Significant effect of sediment cohesion on deltamorphology, Nature Geoscience, 3, 105–109, https://doi.org/10.1038/ngeo730, 2010.

Edmonds, D. A., Paola, C., Hoyal, D. C., and Sheets, B. A.: Quantitative metrics that describe river deltas and their channel networks, Journal of Geophysical Research: Earth Surface, 116, F04 022, https://doi.org/10.1029/2010JF001955, 2011.

Edmonds, D. A., Caldwell, R. L., Brondizio, E. S., and Siani, S. M.: Coastal flooding will disproportionately impact people on river deltas, Nature Communications, 11, 1–8, https://doi.org/10.1038/s41467-020-18531-4, 2020.

Ellery, W. N. and McCarthy, T. S.: Environmental change over two decades since dredging and excavation of the lower Boro River, Okavango Delta, Botswana, Journal of Biogeography, 25, 361–378, https://doi.org/10.1046/j.1365-2699.1998.252168.x, 1998.

Esposito, C. R., Georgiou, I. Y., and Straub, K. M.: Flow Loss in Deltaic Distributaries: Impacts on Channel Hydraulics, Morphology, and Stability, Water Resources Research, 56, e2019WR026 463, https://doi.org/10.1029/2019WR026463, 2020.

Galloway, W. E.: Process framework for describing the morphologic and stratigraphic evolution of deltaic systems, in: Deltas, Models for Exploration, pp. 87–98, Houston Geological Society, 1975.

Geleynse, N., Storms, J. E., Walstra, D. J. R., Jagers, H. R., Wang, Z. B., and Stive, M. J.: Controls on river delta formation; insights from numerical modelling, Earth and Planetary Science Letters, 302, 217–226, https://doi.org/10.1016/j.epsl.2010.12.013, 2011.

Hariharan, J., Wright, K., and Passalacqua, P.: dorado: A Python package for simulating passive particle transport in shallow-water flows, Journal of Open Source Software, 5, 2585, https://doi.org/10.21105/joss.02585, 2020.

Hariharan, J., Xu, Z., Michael, H. A., Paola, C., Steel, E., and Passalacqua, P.: Linking the Surface and Subsurface in River Deltas—Part 1: Relating Surface and Subsurface Geometries, Water Resources Research, 57, e2020WR029 282, https://doi.org/10.1029/2020WR029282, 2021.

Hiatt, M. and Passalacqua, P.: Hydrological connectivity in river deltas: The first-order importance of channel-island exchange, Water Resources Research, 51, 2264–2282, https://doi.org/10.1002/2014WR016149, 2015.

Hiatt, M., Castañeda-Moya, E., Twilley, R., Hodges, B. R., and Passalacqua, P.: Channel-Island Connectivity Affects Water Exposure Time Distributions in a Coastal River Delta, Water Resources Research, 54, 2212–2232, https://doi.org/10.1002/2017WR021289, 2018.

Higgins, S. A., Overeem, I., Rogers, K. G., and Kalina, E. A.: River linking in India: Downstream impacts on water discharge and suspended sediment transport to deltas, Elementa, 6, https://doi.org/10.1525/elementa.269, 2018.

Hoyal, D. C. and Sheets, B. A.: Morphodynamic evolution of experimental cohesive deltas, Journal of Geophysical Research: Earth Surface, 114, 2009, https://doi.org/10.1029/2007JF000882, 2009.

Kain, C. L., Lewarn, B., Rigby, E. H., and Mazengarb, C.: Tsunami Inundation and Maritime Hazard Modelling for a Maximum Credible Tsunami Scenario in Southeast Tasmania, Australia, Pure and Applied Geophysics, 177, 1549–1568, https://doi.org/10.1007/s00024-019-02384-0, 2020.

Kerner, M.: Effects of deepening the Elbe Estuary on sediment regime and water quality, Estuarine, Coastal and Shelf Science, 75, 492–500, https://doi.org/10.1016/j.ecss.2007.05.033, 2007.

Khadim, F. K., Kar, K. K., Halder, P. K., Rahman, M. A., and Morshed, A. M.: Integrated Water Resources Management (IWRM) Impacts in South West Coastal Zone of Bangladesh and Fact-Finding on Tidal River Management (TRM), Journal of Water Resource and Protection, 05, 953–961, https://doi.org/10.4236/jwarp.2013.510098, 2013.

https://doi.org/10.5194/esurf-2022-66
Preprint. Discussion started: 5 December 2022

Knights, D., Sawyer, A. H., Barnes, R. T., Piliouras, A., Schwenk, J., Edmonds, D. A., and Brown, A. M.: Nitrate Removal Across Ecogeomorphic Zones in Wax Lake Delta, Louisiana (USA), Water Resources Research, 56, e2019WR026 867, https://doi.org/10.1029/2019WR026867, 2020.

Lauzon, R. and Murray, A. B.: Comparing the Cohesive Effects of Mud and Vegetation on Delta Evolution, Geophysical Research Letters, 45, 10,437–10,445, https://doi.org/10.1029/2018GL079405, 2018.

Lauzon, R., Piliouras, A., and Rowland, J. C.: Ice and Permafrost Effects on Delta Morphology and Channel Dynamics, Geophysical Research Letters, 46, 6574–6582, https://doi.org/10.1029/2019GL082792, 2019.

Le, T. V. H., Nguyen, H. N., Wolanski, E., Tran, T. C., and Haruyama, S.: The combined impact on the flooding in Vietnam's Mekong River delta of local man-made structures, sea level rise, and dams upstream in the river catchment, Estuarine, Coastal and Shelf Science, 71, 110–116, https://doi.org/10.1016/j.ecss.2006.08.021, 2007.

Lexartza-Artza, I. and Wainwright, J.: Hydrological connectivity: Linking concepts with practical implications, Catena, 79, 146–152, https://doi.org/10.1016/j.catena.2009.07.001, 2009.

Liang, M., Voller, V. R., and Paola, C.: A reduced-complexity model for river delta formation - Part 1: Modeling deltas with channel dynamics, Earth Surface Dynamics, 3, 67–86, https://doi.org/10.5194/esurf-3-67-2015, 2015.

Liang, M., Kim, W., and Passalacqua, P.: How much subsidence is enough to change the morphology of river deltas?, Geophysical Research Letters, 43, 10,266–10,276, https://doi.org/10.1002/2016GL070519, 2016a.

Liang, M., Van Dyk, C., and Passalacqua, P.: Quantifying the patterns and dynamics of river deltas under conditions of steady forcing and relative sea level rise, Journal of Geophysical Research: Earth Surface, 121, 465–496, https://doi.org/10.1002/2015JF003653, 2016b.

Maneewongvatana, S. and Mount, D. M.: Analysis of approximate nearest neighbor searching with clustered point sets, arXiv preprint cs/9901013, 1999.

Masud, M. M. A., Moni, N. N., Azadi, H., and Van Passel, S.: Sustainability impacts of tidal river management: Towards a conceptual framework, Ecological Indicators, 85, 451–467, https://doi.org/10.1016/j.ecolind.2017.10.022, 2018.

Monge-Ganuzas, M., Cearreta, A., and Evans, G.: Morphodynamic consequences of dredging and dumping activities along the lower Oka estuary (Urdaibai Biosphere Reserve, southeastern Bay of Biscay, Spain), Ocean and Coastal Management, 77, 40–49, https://doi.org/10.1016/j.ocecoaman.2012.02.006, 2013.

Moodie, A., Hariharan, J., Barefoot, E., and Passalacqua, P.: pyDeltaRCM: a flexible numerical delta model, Journal of Open Source Software, 6, 3398, https://doi.org/10.21105/joss.03398, 2021.

Moodie, A. J. and Passalacqua, P.: When Does Faulting-Induced Subsidence Drive Distributary Network Reorganization?, Geophysical Research Letters, 48, e2021GL095 053, https://doi.org/10.1029/2021GL095053, 2021.

Mossa, J. and Chen, Y. H.: Geomorphic insights from eroding dredge spoil mounds impacting channel morphology, Geomorphology, 376, 107 571, https://doi.org/10.1016/j.geomorph.2020.107571, 2021.

Nielsen, O., Roberts, S., Gray, D., McPherson, A., and Hitchman, A.: Hydrodynamic modelling of coastal inundation, MODSIM 2005 International Congress on Modelling and Simulation, pp. 518–523, 2005.

Ohimain, E.: Environmental impacts of dredging in the niger delta, Habitat, pp. 9–19, 1996.

Olliver, E. A. and Edmonds, D. A.: Hydrological Connectivity Controls Magnitude and Distribution of Sediment Deposition Within the Deltaic Islands of Wax Lake Delta, LA, USA, Journal of Geophysical Research: Earth Surface, 126, e2021JF006 136, https://doi.org/10.1029/2021JF006136, 2021.

https://doi.org/10.5194/esurf-2022-66
Preprint. Discussion started: 5 December 2022

Olliver, E. A., Edmonds, D. A., and Shaw, J. B.: Influence of Floods, Tides, and Vegetation on Sediment Retention in Wax Lake Delta, Louisiana, USA, Journal of Geophysical Research: Earth Surface, 125, e2019JF005 316, https://doi.org/10.1029/2019JF005316, 2020.

Olson, K. R. and Wright Morton, L.: Polders, dikes, canals, rice, and aquaculture in the Mekong Delta, Journal of Soil and Water Conservation, 73, 83A–89A, https://doi.org/10.2489/jswc.73.4.83A, 2018.

Passalacqua, P.: The Delta Connectome: A network-based framework for studying connectivity in river deltas, Geomorphology, 277, 50–62, https://doi.org/10.1016/j.geomorph.2016.04.001, 2017.

Passalacqua, P., Giosan, L., Goodbred, S., and Overeem, I.: Stable $\neq$ Sustainable: Delta dynamics versus the human need for stability, Earth's Future, p. e2021EF002121, https://doi.org/10.1029/2021EF002121, 2021.

Pethick, J. and Orford, J. D.: Rapid rise in effective sea-level in southwest Bangladesh: Its causes and contemporary rates, Global and Planetary Change, 111, 237–245, https://doi.org/10.1016/j.gloplacha.2013.09.019, 2013.

Piliouras, A., Kim, W., and Carlson, B.: Balancing Aggradation and Progradation on a Vegetated Delta: The Importance of Fluctuating Discharge in Depositional Systems, Journal of Geophysical Research: Earth Surface, 122, 1882–1900, https://doi.org/10.1002/2017JF004378, 2017.

Piliouras, A., Lauzon, R., and Rowland, J. C.: Unraveling the Combined Effects of Ice and Permafrost on Arctic Delta Morphodynamics, Journal of Geophysical Research: Earth Surface, 126, e2020JF005 706, https://doi.org/10.1029/2020JF005706, 2021.

Pringle, C.: The need for a more predictive understanding of hydrologic connectivity, https://doi.org/10.1002/aqc.603, 2003.

Proehl, J. A., Bilgili, A., Lynch, D. R., Smith, K., and Robinson Swift, M.: The use of Lagrangian particle methods to investigate ocean-estuary exchange in well-mixed estuaries, Developments in Water Science, 55, 1825–1837, https://doi.org/10.1016/S0167-5648(04)80188-6, 2004.

Renaud, F. G., Syvitski, J. P., Sebesvari, Z., Werners, S. E., Kremer, H., Kuenzer, C., Ramesh, R., Jeuken, A., and Friedrich, J.: Tipping from the Holocene to the Anthropocene: How threatened are major world deltas?, Current Opinion in Environmental Sustainability, 5, 644–654, https://doi.org/10.1016/j.cosust.2013.11.007, 2013.

Roberts, S., Nielsen, O., Gray, D., Sexton, J., and Davies, G.: ANUGA User Manual, 2015.

Roberts, S. G., Stals, L., and Nielsen, O. M.: Parallelisation of a finite volume method for hydrodynamic inundation modelling, ANZIAM Journal, 49, 558, https://doi.org/10.21914/anziamj.v48i0.153, 2007.

Samuelson, B. M.: THE EFFECT OF FLOOD EMBANKMENTS ON THE RIVER-LEVELS IN THE IRRAWADDY DELTA.(ABRIDGES)., in: Minutes of the Proceedings of the Institution of Civil Engineers, vol. 203, pp. 362–370, Thomas Telford-ICE Virtual Library, 1917.

Sassi, M. G., Hoitink, A. J., De Brye, B., Vermeulen, B., and Deleersnijder, E.: Tidal impact on the division of river discharge over distributary channels in the Mahakam Delta, Ocean Dynamics, 61, 2211–2228, https://doi.org/10.1007/s10236-011-0473-9, 2011.

Sassi, M. G., Hoitink, A. J., De Brye, B., and Deleersnijder, E.: Downstream hydraulic geometry of a tidally influenced river delta, Journal of Geophysical Research F: Earth Surface, 117, 4022, https://doi.org/10.1029/2012JF002448, 2012.

Sendrowski, A. and Passalacqua, P.: Process connectivity in a naturally prograding river delta, Water Resources Research, 53, 1841–1863, https://doi.org/10.1002/2016WR019768, 2017.

Shaw, J. B., Wolinsky, M. A., Paola, C., and Voller, V. R.: An image-based method for shoreline mapping on complex coasts, Geophysical Research Letters, 35, n/a–n/a, https://doi.org/10.1029/2008GL033963, 2008.

Shaw, J. B., Mohrig, D., and Wagner, R. W.: Flow patterns and morphology of a prograding river delta, Journal of Geophysical Research: Earth Surface, 121, 372–391, https://doi.org/10.1002/2015JF003570, 2016.

https://doi.org/10.5194/esurf-2022-66
Preprint. Discussion started: 5 December 2022

Simeoni, U. and Corbau, C.: A review of the Delta Po evolution (Italy) related to climatic changes and human impacts, Geomorphology, 107, 64–71, https://doi.org/10.1016/j.geomorph.2008.11.004, 2009.

Straub, K. M., Li, Q., and Benson, W. M.: Influence of sediment cohesion on deltaic shoreline dynamics and bulk sediment retention: A laboratory study, Geophysical Research Letters, 42, 9808–9815, https://doi.org/10.1002/2015GL066131, 2015.

Temmerman, S. and Kirwan, M. L.: Building land with a rising sea, Science, 349, 588–589, 2015.

Tetzlaff, D., Soulsby, C., Bacon, P. J., Youngson, A. F., Gibbins, C., and Malcolm, I. A.: Connectivity between landscapes and riverscapes - A unifying theme in integrating hydrology and ecology in catchment science?, https://doi.org/10.1002/hyp.6701, 2007.

Tull, N., Passalacqua, P., Hassenruck-Gudipati, H. J., Rahman, S., Wright, K., Hariharan, J., and Mohrig, D.: Bidirectional River-Floodplain Connectivity During Combined Pluvial-Fluvial Events, Water Resources Research, 58, e2021WR030 492, https://doi.org/10.1029/2021wr030492, 2022.

Vale, L. M. and Dias, J. M.: Coupling of a Lagrangian particle tracking module to a numerical hydrodynamic model: Simulation of pollution events inside an estuarine port area, Journal of Coastal Research, pp. 1609–1613, 2011.

Valseth, E., Loveland, M. D., Dawson, C., and Buskey, E. J.: A study of the potential impact of dredging the corpus christi ship channel on passive particle transport, Journal of Marine Science and Engineering, 9, 935, https://doi.org/10.3390/jmse9090935, 2021.

van der Walt, S., Schönberger, J. L., Nunez-Iglesias, J., Boulogne, F., Warner, J. D., Yager, N., Gouillart, E., Yu, T., and scikit-image contributors, T.: scikit-image: image processing in Python, PeerJ, 2, e453, https://doi.org/10.7717/peerj.453, 2014.

van Dijk, W. M., Cox, J. R., Leuven, J. R., Cleveringa, J., Taal, M., Hiatt, M. R., Sonke, W., Verbeek, K., Speckmann, B., and Kleinhans, M. G.: The vulnerability of tidal flats and multi-channel estuaries to dredging and disposal, Anthropocene Coasts, 4, 36–60, https://doi.org/10.1139/anc-2020-0006, 2021.

Viero, D. P. and Defina, A.: Water age, exposure time, and local flushing time in semi-enclosed, tidal basins with negligible freshwater inflow, Journal of Marine Systems, 156, 16–29, https://doi.org/10.1016/j.jmarsys.2015.11.006, 2016.

Virtanen, P., Gommers, R., Oliphant, T. E., Haberland, M., Reddy, T., Cournapeau, D., Burovski, E., Peterson, P., Weckesser, W., Bright, J., van der Walt, S. J., Brett, M., Wilson, J., Millman, K. J., Mayorov, N., Nelson, A. R. J., Jones, E., Kern, R., Larson, E., Carey, C. J., Polat, I., Feng, Y., Moore, E. W., VanderPlas, J., Laxalde, D., Perktold, J., Cimrman, R., Henriksen, I., Quintero, E. A., Harris, C. R., Archibald, A. M., Ribeiro, A. H., Pedregosa, F., van Mulbregt, P., and SciPy 1.0 Contributors: SciPy 1.0: Fundamental Algorithms for Scientific Computing in Python, Nature Methods, 17, 261–272, https://doi.org/10.1038/s41592-019-0686-2, 2020.

Wang, X., Zhang, W., Yin, J., Wang, J., Ge, J., Wu, J., Luo, W., and Lam, N. S.: Assessment of coastal erosion vulnerability and socio-economic impact along the Yangtze River Delta, Ocean and Coastal Management, 215, 105 953, https://doi.org/10.1016/j.ocecoaman.2021.105953, 2021.

Wesselink, A., Warner, J., Syed, M. A., Chan, F., Tran, D. D., Huq, H., Huthoff, F., Le Thuy, N., Pinter, N., Van Staveren, M., and Others: Trends in flood risk management in deltas around the world: Are we going 'soft'?, International Journal of Water Governance, 3, 25–46, 2015.

Wilson, C., Goodbred, S., Small, C., Gilligan, J., Sams, S., Mallick, B., and Hale, R.: Widespread infilling of tidal channels and navigable waterways in the human-modified tidal deltaplain of southwest Bangladesh, Elementa, 5, https://doi.org/10.1525/elementa.263, 2017.

Wright, K., Hariharan, J., Passalacqua, P., Salter, G., and Lamb, M. P.: From Grains to Plastics: Modeling Nourishment Patterns and Hydraulic Sorting of Fluvially Transported Materials in Deltas, Journal of Geophysical Research: Earth Surface, p. e2022JF006769, https://doi.org/https://doi.org/10.1029/2022JF006769.

https://doi.org/10.5194/esurf-2022-66
Preprint. Discussion started: 5 December 2022

Wright, K., Passalacqua, P., Simard, M., and Jones, C. E.: Integrating Connectivity Into Hydrodynamic Models: An Automated Open-Source Method to Refine an Unstructured Mesh Using Remote Sensing, Journal of Advances in Modeling Earth Systems, 14, e2022MS003 025, https://doi.org/https://doi.org/10.1029/2022MS003025, e2022MS003025 2022MS003025, 2022.

Yuan, R. and Zhu, J.: The Effects of Dredging on Tidal Range and Saltwater Intrusion in the Pearl River Estuary, Journal of Coastal Research, 31, 1357–1362, https://doi.org/10.2112/JCOASTRES-D-14-00224.1, 2015.

Zhu, J., Weisberg, R. H., Zheng, L., and Han, S.: Influences of Channel Deepening and Widening on the Tidal and Nontidal Circulations of Tampa Bay, Estuaries and Coasts, 38, 132–150, https://doi.org/10.1007/s12237-014-9815-4, 2015.

Zoccarato, C., Minderhoud, P. S., and Teatini, P.: The role of sedimentation and natural compaction in a prograding delta: insights from the mega Mekong delta, Vietnam, Scientific Reports, 8, 1–12, https://doi.org/10.1038/s41598-018-29734-7, 2018.

https://doi.org/10.5194/esurf-2022-66
Preprint. Discussion started: 5 December 2022

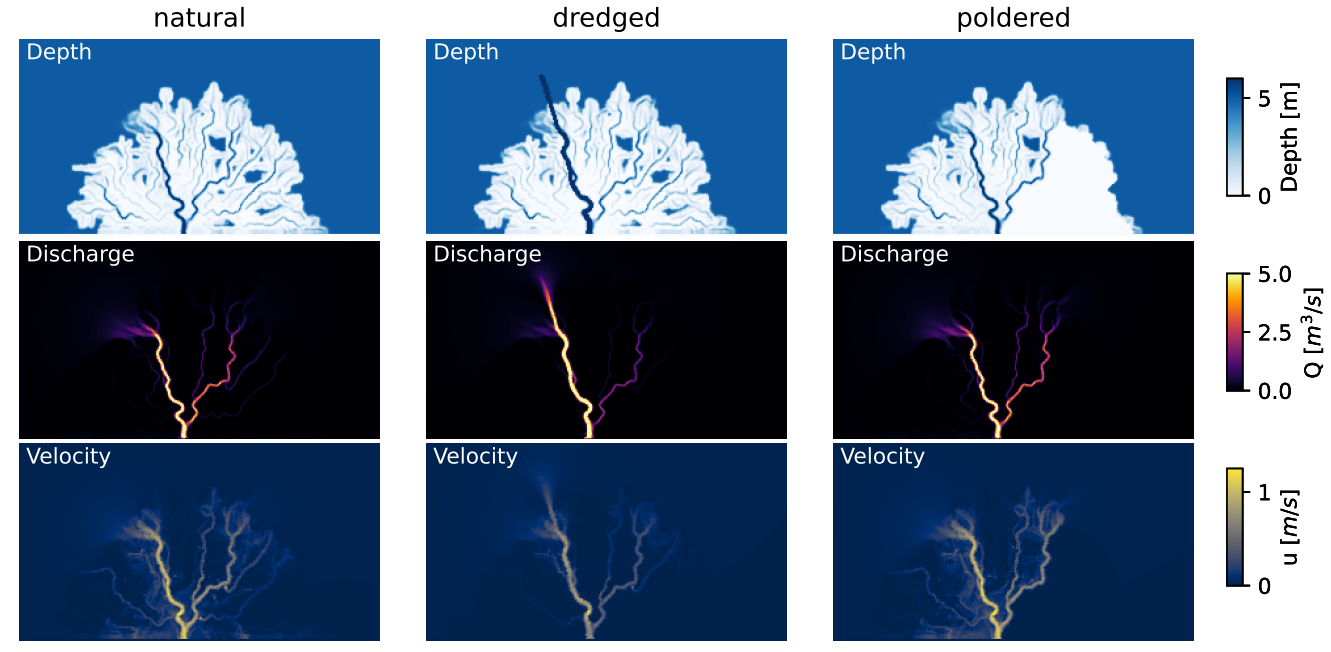

Figure A1. Example of ANUGA steady flow fields over three topographies.

https://doi.org/10.5194/esurf-2022-66
Preprint. Discussion started: 5 December 2022

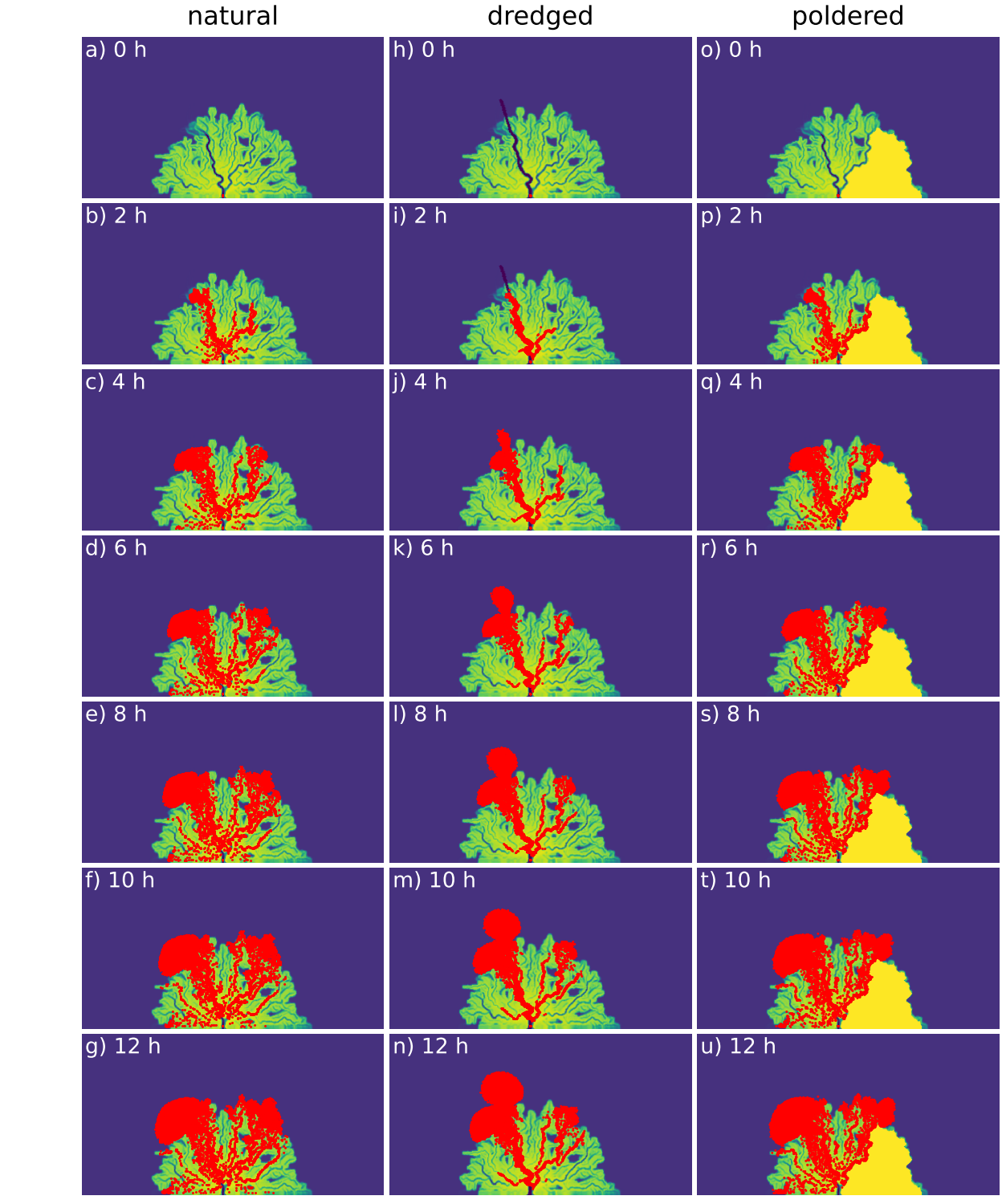

Figure A2. Examples of particle movement ($\theta = 1$) across three topographies shown as still images every 2 hours for the first 12 hours of their movement under steady flow conditions.

https://doi.org/10.5194/esurf-2022-66
Preprint. Discussion started: 5 December 2022

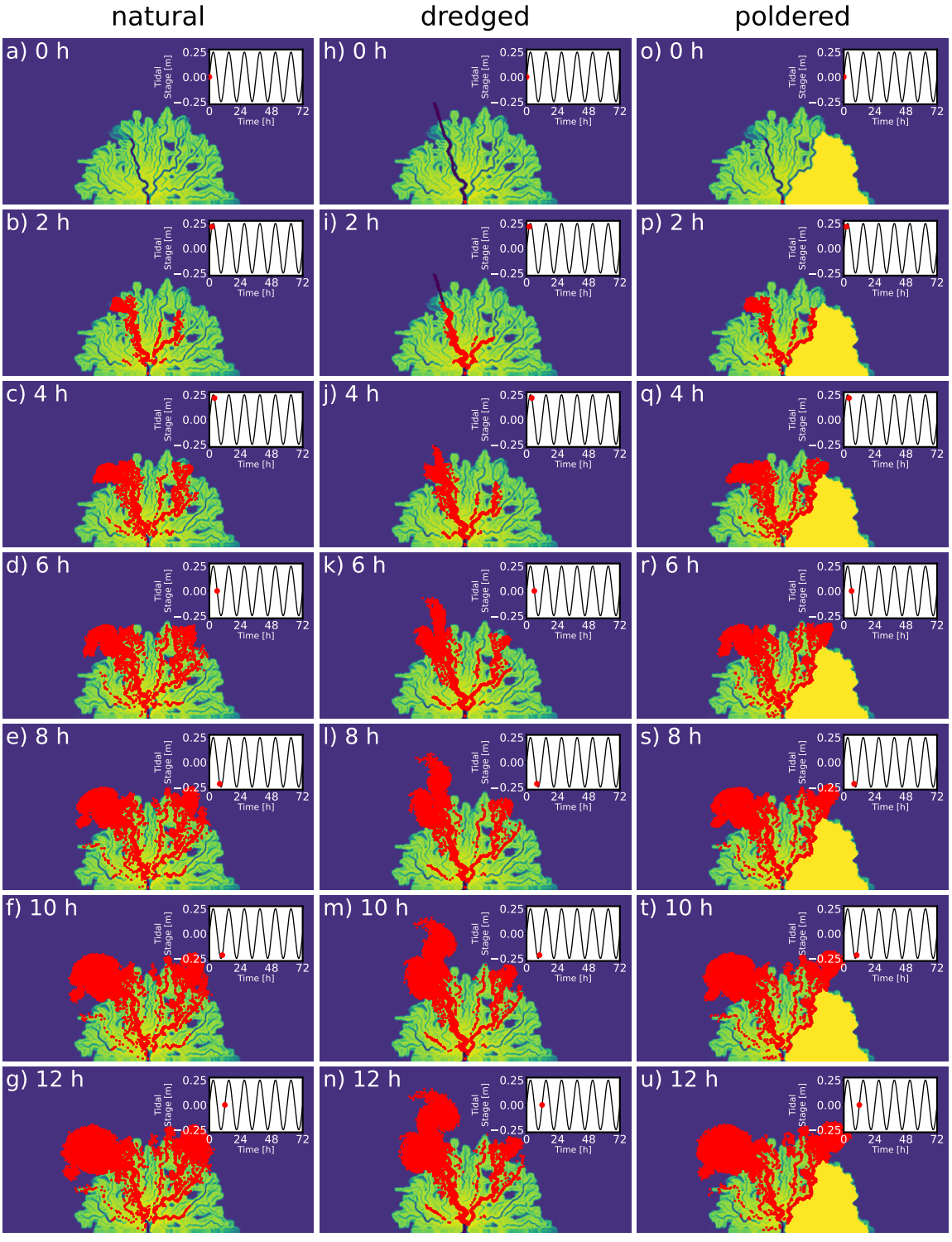

Figure A3. Examples of particle movement ($\theta = 1$) across three topographies shown as still images every 2 hours for the first 12 hours of their movement under unsteady (tidal) flow conditions.

https://doi.org/10.5194/esurf-2022-66
Preprint. Discussion started: 5 December 2022

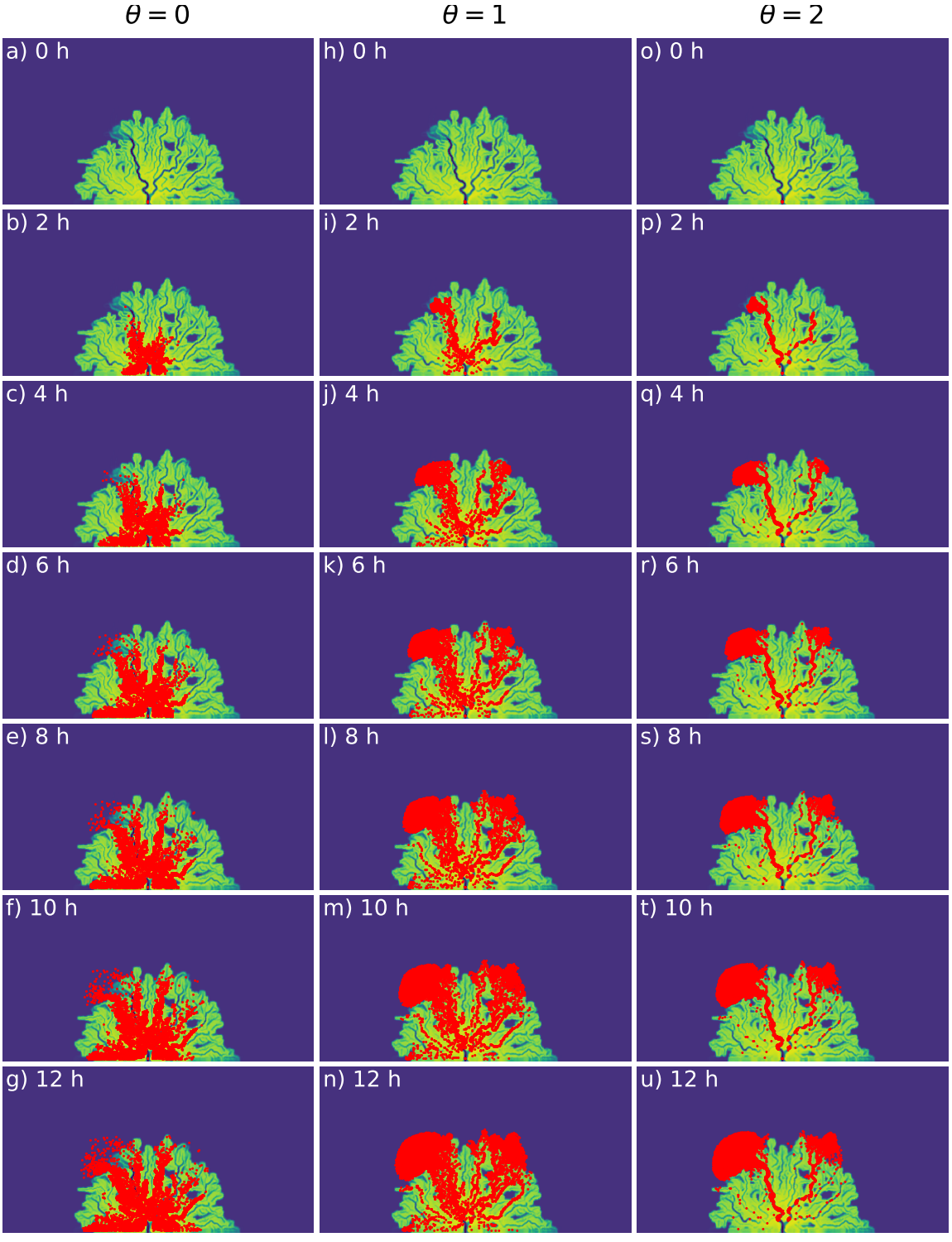

Figure A4. Examples of particle movement with three different θ values across natural topography shown as still images every 2 hours for the first 12 hours of their movement under steady flow conditions.

https://doi.org/10.5194/esurf-2022-66
Preprint. Discussion started: 5 December 2022

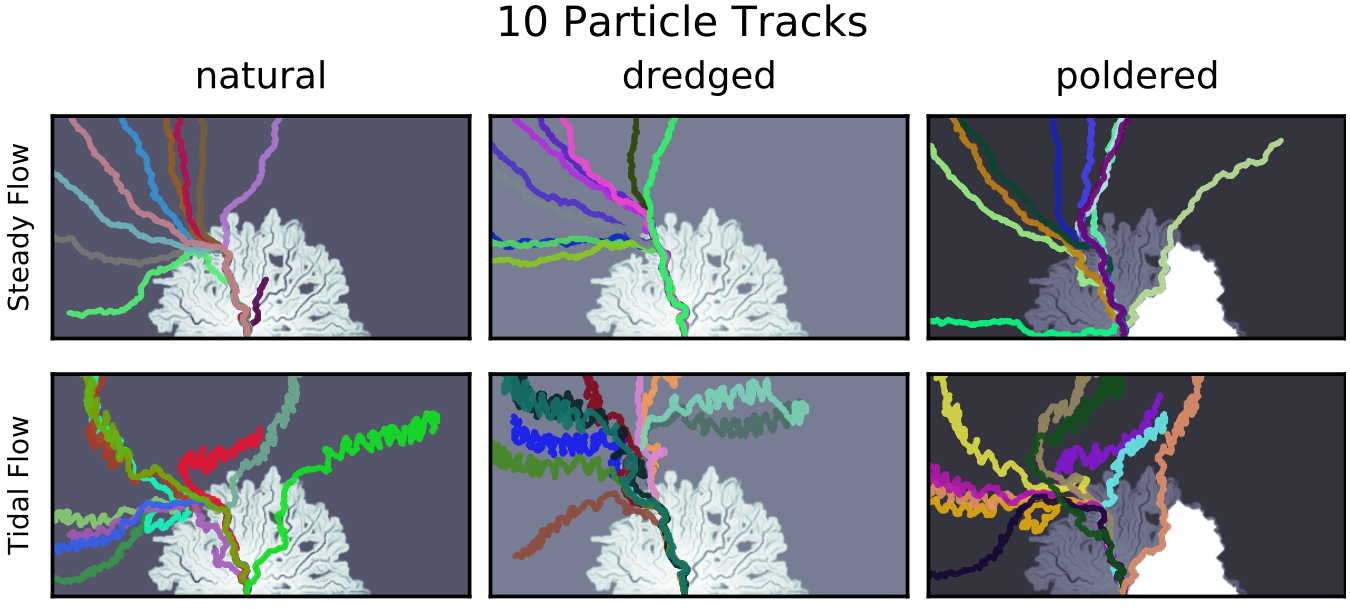

Figure A5. Examples of 10 particle tracks over three different topographies under steady and tidal flow conditions.

https://doi.org/10.5194/esurf-2022-66
Preprint. Discussion started: 5 December 2022

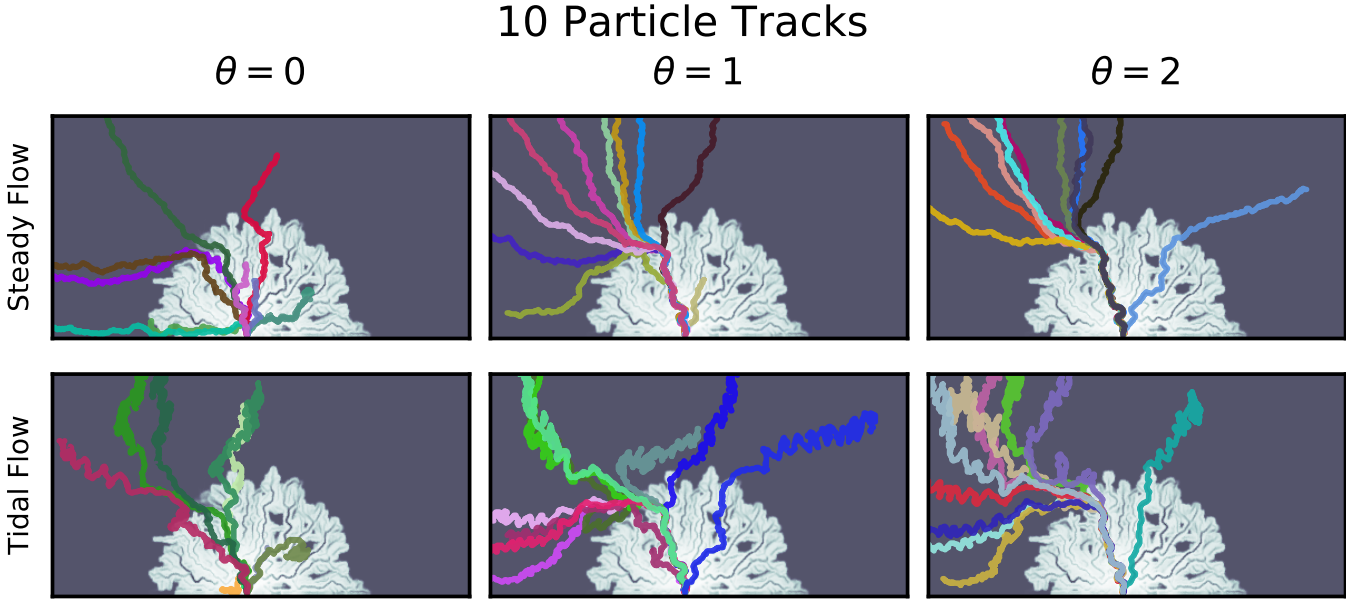

Figure A6. Examples of 10 particle tracks with different θ values over a natural topography under steady and tidal flow conditions.

https://doi.org/10.5194/esurf-2022-66
Preprint. Discussion started: 5 December 2022

Earth Surface Dynamics Discussions
Open Access
EGU

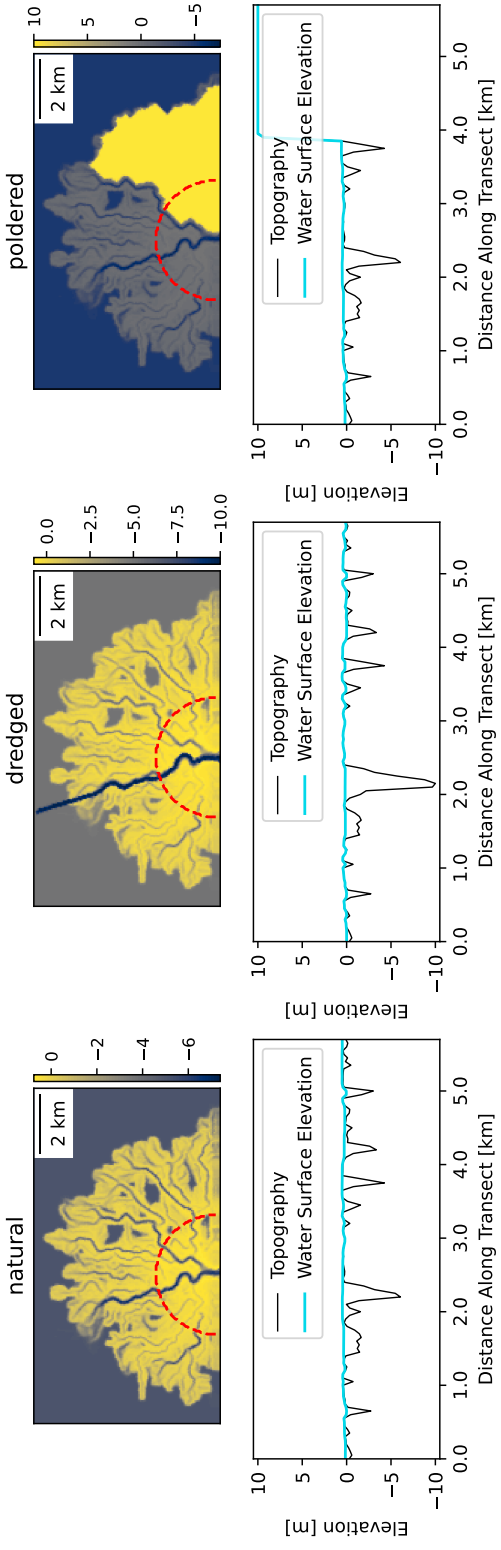

Figure A7. Example circular sections with radii of 2 km through natural, dredged, and poldered topographies for a single model run ($f_{sand} = 0.25$).

https://doi.org/10.5194/esurf-2022-66
Preprint. Discussion started: 5 December 2022

Table A1. Polder areas in square kilometers for each of the 6 model replicates for each of the 3 input sand scenarios.

$f_{sand} = 0.25$	$f_{sand} = 0.50$	$f_{sand} = 0.75$
12.55	6.3475	11.755
14.69	19.4825	9.4875
12.67	11.735	25.445
15.785	12.7325	9.4125
20.085	14.5675	19.19
11.9975	7.3175	11.3325

https://doi.org/10.5194/esurf-2022-66
Preprint. Discussion started: 5 December 2022

Table A2. Dredge channel areas in square kilometers for each of the 6 model replicates for each of the 3 input sand scenarios.

$f_{sand} = 0.25$	$f_{sand} = 0.50$	$f_{sand} = 0.75$
0.955	1.0475	1.0025
1.005	0.8775	0.98
1.0725	1.0025	0.965
1.0825	0.9775	1.03
1.1325	0.9625	0.9725
1.005	1.0075	0.9575

https://doi.org/10.5194/esurf-2022-66
Preprint. Discussion started: 5 December 2022


Earth Surface Dynamics Discussions
Open Access
EGU

Table A3. Edge length statistics (minimum, percentile values in increments of 10, and maximum, in meters) for the triangles in the ANUGA mesh.

Min.	10%	20%	30%	40%	50%	60%	70%	80%	90%	Max.
27.36	38.04	39.72	41.22	42.71	44.23	45.78	47.59	49.75	52.27	9338.5